Observational Study on Multiscale Structures of Line-Shaped Precipitation Bands

東, 邦昭

(Degree)
博士 (理学)
(Date of Degree)
2009-03-25
(Date of Publication)
2009-10-15
(Resource Type)
doctoral thesis
(Report Number)
甲4521
(URL)
https://hdl.handle.net/20.500.14094/D1004521

Doctoral Dissertation

Observational Study on Multiscale Structures of Line-Shaped Precipitation Bands

January 2009

Graduate School of Science and Technology, Kobe University

Kuniaki Higashi

博士論文

Observational Study on Multiscale Structures of Line-Shaped Precipitation Bands

(線状降水帯のマルチスケール構造に関する観測的研究)

平成 21 年 1 月

神戸大学大学院自然科学研究科

東　邦昭

Acknowledgements

The author wishes to express his sincere appreciation to Professor Manabu D. Yamanaka for his continuous encouragement, helpful leads to finding the scientific importance, giving many opportunities to participate international observation and domestic conferences and supervision in the present work.

The author is grateful to Professor Yoshi-Yuki Hayashi, Professor Shin-Ya Ogino and Professor Tadashi Mukai for his adequate and importance comments for establishment of the purposes and presentations of the present work.

The author owes Professor Emeritus Takeshi Fujii for many helpful suggestions concerning the way to advance the present work and using laboratory of Kyoto Sangyo University. Under his supervision the author's Bachelor Thesis (2003) and Master Thesis (2005) were submitted and accepted, and contexts of them are extended and involved in this Doctoral Thesis.

The author deeply thanks Professor Yoshiaki Shibagaki for many useful discussions concerning the way to advance the present work. The author deeply thanks Mr. Yasutomo Kiyohara for his kind guidance for numerical model technique, rawinsonde observations, and technical support regarding computer hardware and software, and many helpful valuable suggestions. Special thanks are due to Mr. Masanori Kusuda for his many valuable comments concerning the way to advance the present work.

The author is grateful to Professor Takahiro Iwayama, Dr. George L. Hashimoto and Dr. Yoshiyuki O. Takahashi for their adequate and important comments of the present work.

The author deeply thanks Professor Hiroyuki Hashiguchi, Dr. Michihiro Teshiba, Dr. Yasuko Umemoto, Dr. Ryuzo Araki and Mr. Shunsuke Tsushima for their leadership to conduct intensive rawinsonde observations successfully and who gave many useful discussions.

The author is grateful to Dr. Hiromu Seko of Meteorological Research Institute (MRI), Professor Ikuo S. Sogami of Kyoto Sangyo University, Dr. Masato Nodzu of Research Institute for Humanity and Nature, and Mr. Satoshi Matsumura of Osaka District Meteorological Observatory for their constructive comments.

The author thanks members of the Research Institute for Sustainable Humanosphere (RISH), Kyoto University for operation of rawinsonde observations at the MU Radar Observatory, and Hydrospheric Atmospheric Research Center (HyARC), Nagoya University for providing a receiver for rawinsonde observation system.

The author acknowledges Japan Meteorological Agency (JMA) for their providing the data of objective analysis, wind profilers, and AMeDAS stations data.

Abstract

In Kinki District of the central Japan, line-shaped precipitation bands (width ≈ 20 km, length ≈ 100 km) are often found. Those precipitation bands have been noted in operational meteorological observatories and some laboratories because the bands are abruptly formed around Osaka Bay, and bring large amount of precipitation (about 70 mm h^{-1}). In general such a line-shaped convective system is in the order of 100 km in length, 10 km at width and height. The life time is a few hours. We consider the smaller hierarchical structures exist around precipitation bands, because some mountains exist in Kinki District (e.g. Mt. Rokko, Awaji Island, Mt. Izumi and Mts. Kii). These studies have not been performed. In this thesis, we investigate the reason why the line-shaped precipitation bands were formed or intensified around Osaka Bay in Baiu season in detail to use own observation data, some Japan Meteorological Agency (JMA) data, and numerical model (see Chapter 2).

We performed the climatological analysis for line-shaped precipitation band. When the wind direction is southerly, the line-shaped precipitation band is formed easily for the other wind directions. When the southerly is less than 10 m s^{-1}, the band like precipitation band is not seen to around Osaka Bay. But when the southerly is more than 10 m s^{-1}, we appear the band like structure. These results are consistent with previous case studies. The band like precipitation peak is distinguished, when the southerly is between 20–25 m s^{-1}. Therefore, we consider that the strong southerly (about 20 m s^{-1}) is one of the conditions of formed the intense line-shaped precipitation band around Osaka Bay (see Chapter 3).

Conditionally (convectively) unstable stratification (θ_e > 345 K at 950-hPa level, and < 335 K at 600-hPa level where moisture was less than 5 g kg^{-1}) appeared near the cold front passing Osaka Bay. The line-shaped precipitation band was generated in warm air in front of the cold front. It was located in the convergence zone between southwesterly from Kii Channel and westerly on the western (cold) side of cold front in the lower layer (below 900-hPa level). In the middle troposphere (~ 700-hPa level), strong westerly (20–30 m s^{-1}) corresponding to Baiu jet was also dominant over the precipitation band. As the cold front approached Kinki District, a meso-β-scale wave was formed from Shikoku Island to Kii Peninsula. According to the development of the wave, the Tokushima small low formed in a deep trough of the wave, located in the eastern part of Shikoku Island. Its life time was about 6 hours. When the line-shaped precipitation band was observed, the southerly over Kii Channel was intensified (about 15 m s^{-1}) by Tokushima small low in the lower layer (< 900-hPa level). This southerly and the westerly corresponding to Baiu jet produced a vertical wind shear with clockwise rotation with height from surface to 700-hPa level, which is a suitable condition for development of the line-shaped precipitation band. The origin of the Tokushima small low is not considered to be thermal but hydrodynamic due to Shikoku Mountains. Westerly in the western side of the cold front passed over the mountains of Awaji Island and caused lee waves. The meso-γ-scale lee waves triggered active precipitation clouds in the conditionally unstable atmosphere.

Contents

List of Figures

List of Tables

Chapter 1

General introduction

1.1 Mesoscale convective systems

A mesoscale convective system consist of individual convective storms complexes is a cloud system that occurs in connection with an ensemble of thunderstorms and produces a contiguous precipitation area ～100 km or more in horizontal scale in at least one direction (Houze 1993). The patterns of wind and weather associated with mesoscale convective systems are important local phenomena, which often must be forecasted on short time scales. These systems also produce a large proportion of the earth's precipitation and thus are important climatologically. Mesoscale convective systems occur in a variety of forms. Tropical clouds formed over oceans area in environments which are rather uniform horizontally. The air masses are continuously heated from below, and the convection is always mixing the air vertically. The environment is generally neutral or conditionally unstable. The horizontal uniformity over wide regions is maintained in part because the tropics are relatively unaffected by strong baroclinic waves and fronts such as those that dominate the mid-latitudes. In mid-latitudes, mesoscale convective systems can be entangled with clouds, and precipitation produced by baroclinic and frontal processes, and the purely convective processes thereby become more difficult to be isolated. The precipitation areas of mid-latitude mesoscale convective systems are similar to those in the tropic. That the rain areas are similar size and, at their mature stage of development, consist of a group or line of convective showers embedded in or adjoining a large region of stratiform precipitation.

We have noted that in both the tropics and mid-latitudes, one type of precipitation structure that can occur in a mesoscale convective system is a sharply defined convective line with trailing stratiform precipitation. This structure was shown by examples in Fig. 1.1. This form is so sharply defined that it is more amenable to study and has been examined intensively in a variety of ways. The line-shaped precipitation band is organized into a meso-α-scale disturbance such as stationary and cold fronts (Tatehira and Fukatsu 1963; Hobbs et al. 1980; Matejka et al. 1980). On the other hand, the line-shaped precipitation band is organized meso-γ-scale cumulonimbus whose horizontal scale is 10 km order, and time scale is about 1 hour.

1.2 Features of mesoscale convective systems in Japan

Most of heavy rainfalls including sometimes disasters such as landslides and floods in Japan during the Baiu season, i.e., the period from early June to middle of July, are brought by mesoscale convective systems with line-shaped structures (e.g. Ogura 1991). In general such line-shaped convective systems are in a 100 km horizontal scale in length, and in 10 km scales at width and height. The life time is several hours. These scales are called so meso-β-scale (Orlanski 1975). Satellite and/or weather radar observations are useful to investigate these phenomena. Ninomiya and Akiyama (1992) and Ogura (1997) showed conceptual model of rainfall systems which is classical structure in Baiu season (see Fig. 1.2). Synoptic scale cyclone which specific scale is about 5000 km has several meso-α-scale disturbances. Specific scale of this disturbance is about 1000 km. A meso-α-scale disturbance has several meso-β-scale disturbances, and a meso-β-scale disturbance also has several meso-γ-scale cumulonimbi.

One hand, line-shaped precipitation band is caused by compulsory force as orographic effect. Line-shaped rainfall systems with precipitation stronger than 150 mm day^{-1} observed from June to September in around Kyushu, called Koshikijima and Nagasaki lines were formed when intense southerly or southwesterly wind from tropics in the lower layer with a height of about 1 km was maintained for 12 hours by meso-α-scale cyclone systems (Sato, 1999, private communication; Kato et al. 2003; Tashiro, 2004; Kato, 2005). Sato (1999, private communication) statistically examined the appearance frequency of the Nagasaki line by using observed data of the JMA radar for five years. He also classified it using the wind direction that was observed at the weather station in Mt. Unzen. It is located at a height of about 680 m. A band-shaped rainfall area, with high appearance frequency, was analyzed corresponding to the Nagasaki line, only when the wind direction was found between south-southwest and southwest. Kato (2005) statistically investigated the appearance of the Koshikijima line additional of the Nagasaki line. He used the weather radar and upper air observational data by JMA from 1994 to 2003 in June and July. The JMA data is effective to perform these statistically analysis, however we are not enough to investigate the formation and/or maintenance mechanism of a case. Because the time and spatial resolutions of the JMA data is coarse compared with the mesoscale phenomenon. Umemoto et al. (2004) performed case study to clear maintenance and formation mechanism of Koshikijima line-shaped precipitation band. She used own observed data which is rawinsonde upper air sounding and Doppler radar observation near the line-shaped precipitation band added to the JMA data. In their common results, humid air flowed to the windward of mountain, the air parcel compulsory over level of condensation level and level of free convective level easily.

On the other hand, line-shaped precipitation band is caused in the unstable layer as frontal zone or as tropical cyclone. The frontal zone existed in a high potential temperature gradient. Kato (2006) investigated Fukuoka heavy rainfall on 29 June 1999. The line-shaped precipitation band occurs to the frontal zone where convective instability is strongest in the environmental field. In the other case, we know the precipitation is partial enhanced, because the line-shaped precipitation band has multiscale structures. Yamakawa (1980) showed that a cyclonic circulation in the lowest layer associated with a thermal low transported of warm and moist air to thunderstorms associated with cold fronts passing the central Japan. In Kanto District, Sakakibara (1983) showed that a precipitation system was developed probably due to meso-β-scale lows generated by orography, which intensified warm southerly winds responsible for intense convections near the surface front. These previous case studies concerned convective systems with heavy rainfall in relation meso-α-scale and meso-β-scale systems complexity (e.g., Ninomiya and Akiyama, 1974; Ninomiya, 1978; Ninomiya and Shibagaki 2007).

In Kinki District of the central Japan (see Fig. 2.6), line-shaped precipitation bands (width ≈ 20 km, length ≈ 100 km) are often found. This precipitation band has been interested in JMA and some laboratories because the band is abruptly formed around Osaka Bay, and is brought large amount of precipitation (about 70 mm h^{-1}). Therefore some previous studies performed in JMA and universities. Yokota (1993, private communication) shows this line-shaped precipitation occurred on 11 Sep 1988. He investigated it use to the JMA operational radar and surface weather station data. Fig. 1.3 is shown by characteristic of the precipitation band is organized from Osaka Bay to Osaka plain. The precipitation band was stagnant in this area at least 1 hour. Konishi and Umemoto (2001, private communication) observed 48 rainfall events stronger than 20 mm h^{-1} occurred from Baiu to autumn seasons during 1998–2000 by using their own rain gage network over northern Osaka Plain, and showed that the warm moist air mass were intruded over Kii Channel or Ise Bay before precipitation started. Okumura and Satomura (2001, private communication), and Arai et al. (2001, private communication) used the operational observation network including an X-band Doppler radar and showed that band-like structures appeared near the cold front extended south-ward or southwest-ward from the Sea of Japan to the Honshu Island and westerly wind was dominant in a meso-α-scale area at 3 km altitude. Shibagaki et al. (2000) analyzed a hierarchical structure of meso-β- and -γ-scale cloud systems in the meso-α-scale cyclone during Baiu season using MU radar and meteorological radars. We make clear that the southerly or southwesterly is necessity to form the line-shaped precipitation band around Osaka Bay from these previous case studies. This feature is commonly in Kyusyu area. However when the southerly or southwesterly is dominant in Kii Channel, the line-shaped precipitation band is not sure to form in around Osaka Bay. They consider that the other terms will be necessity to form the band, but the previous operational observation data is limited surface and the upper air observatory is far from formatting the line-shaped precipitation band. Recently we can use to the new observation systems as wind profiler and high resolution analyzed data as mesoscale objective analysis data (MANAL). Further, the mesoscale numerical models (e.g. MM5, WRF, and NHM) are developed, we functional use to support of the observation data. In this thesis, we clarify formative condition of the line-shaped precipitation band to use these newly observation data and numerical model (MM5).

1.3 Structure of thesis

The purpose of this thesis is to investigate the reason why the line-shaped precipitation bands were formed or intensified around Osaka Bay in Baiu season in detail. We will consider all the meso-α-, -β-, and -γ-scales and also orographic effect. In Chapter 2, observation and data description are shown. In Chapter 3, Climatological description of cold front passages as a condition generating the line-shaped precipitation bands over Osaka Bay is given, of which the major part has been published in Higashi and Fujii (2008). Chapter 4 concerns case studies of the organized precipitation band on 15 October 1998, 8 April 2003, 2 July 2006 and 5 July 2006, and

Chapter 5 concerns numerical simulation and discussions on the role of a meso-α scale cyclone and formation of a meso-β scale low. A case of October 1998 has been published in Higashi and Fujii (2004), and the two cases in 2006 and the major part of discussions will be published in Higashi et al. (2008). Chapter 6 is general conclusions of this thesis.

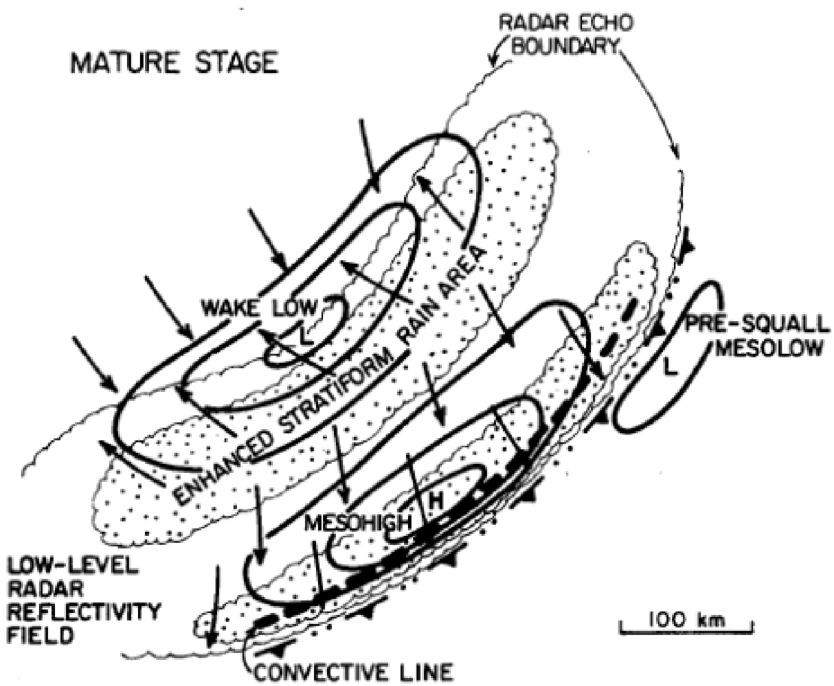

Figure 1.1. Schematic structure of mature stage line-shaped precipitation band (Johnson and Hamilton 1988).

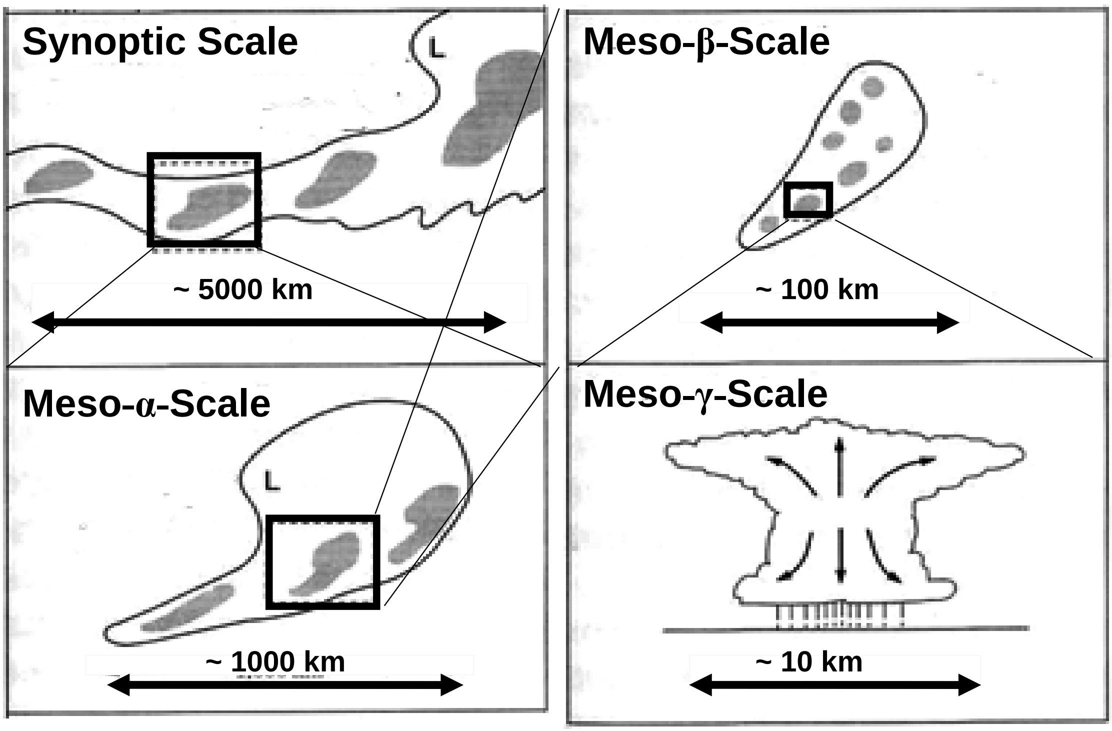

Figure 1.2. Schematic structure of hierarchical structures at rainfall systems edited Akiyama and Ninomiya (1992) and Ogura (1997).

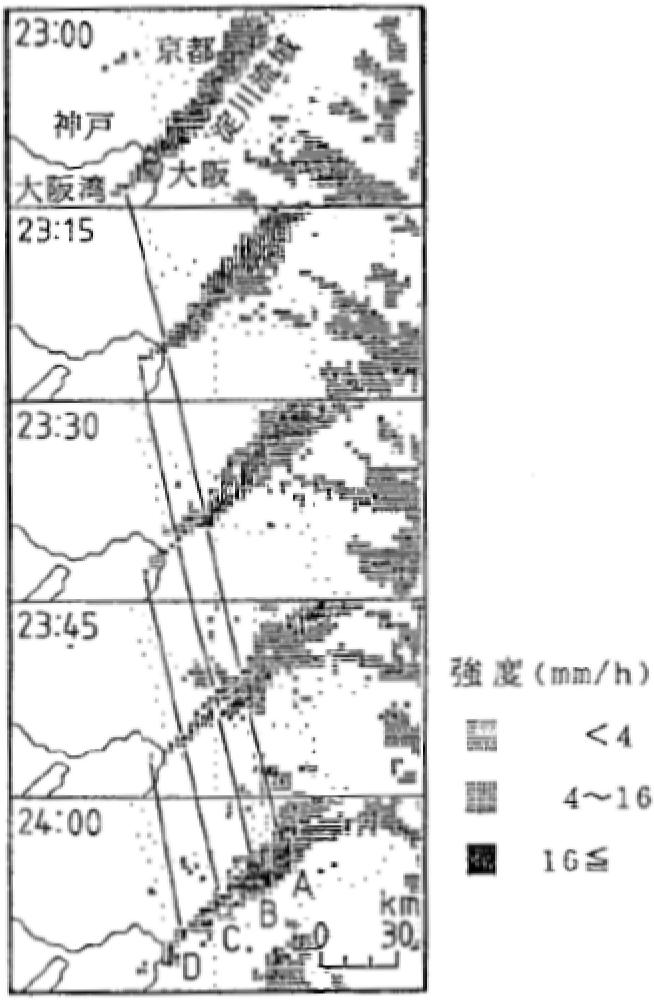

Figure 1.3. JMA radar echo distributions around Osaka Bay from 2300 to 2400 JST on 11 Sep 1988. Shaded area is precipitation intensity (Yokota 1993, private communication).

Chapter 2

Observation and numerical model

2.1 Weather maps

Weather maps are provided by Japan Meteorological Agency (JMA). We used surface, 850- and 500-hPa levels weather maps. The surface weather map is provided for four times (0300, 0900, 1500 and 2100 JST, where JST = UTC + 9 hours) in a day, and the pressure level weather maps are provided for two times (0900 and 2100 JST) in a day.

2.2 Mesoscale objective analysis data

We used the mesoscale objective analysis data (MANAL) provided by JMA. The time interval is 6 hours (at 0300, 0900, 1500 and 1800 JST, where JST = UTC + 9 hours) and 3 hours (at 0000, 0300, 0600, 0900, 1200, 1500, 1800 and 2100 JST) before and after Mar 2006, respectively. The horizontal resolution is 10×10 km. The vertical resolution is 20 layers (1000, 950, 925, 900, 850, 800, 700, 600,500, 400, 300, 250, 200, 150, 100, 70, 50, 30, 20 and 10 hPa) for zonal and meridional wind and temperature, and 11 layers (up to 300-hPa level) for relative humidity. Surface data have sea level pressure, zonal and meridional wind, temperature and relative humidity.

2.3 Surface weather station data

The surface weather data is observed by JMA at Kinki District, whose location are shown in Fig. 2.1. As the environmental field, we used the wind data that was observed at Tomogashima at every hour. Because Tomogashima is located on the Kii Channel, which upstream side of the line-shaped precipitation band in the southerly or southwesterly wind field. The precipitation data is used every hour in Kinki District.

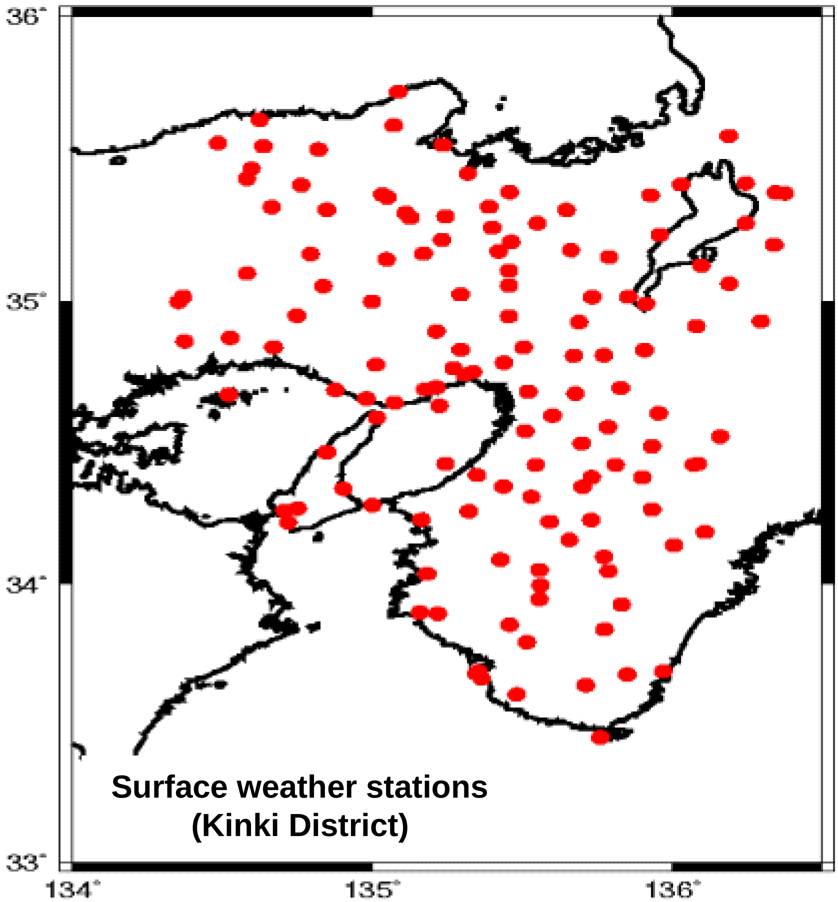

Figure 2.1. Distributions of surface weather stations of JMA in Kinki District.

2.4 Meteorological radar data

Meteorological radar is based on the fact that electromagnetic waves interact with hydrometeors as they propagate through the atmosphere. When they encounter hydrometeors, a small fraction of their energy is scattered by the particles and a detectable amount of power is backscattered to a receiver. Basic radar consists of a transmitter to produce power at a known frequency; an antenna to focus the transmitted waves to a beam about 1°–2° wide and to receive the fraction of the power backscattered from the targets. 5.3 GHz meteorological radars are operated by JMA. Fig. 2.2 shows Osaka Takayasuyama radar site. A constant-altitude plan position indicator (CAPPI) data at 2 km altitude was used to examine a horizontal distribution of precipitating clouds. The observational range is 300 km, and the time interval is 10 minutes. The horizontal resolution is 2.5 km before Jun 2006, and 1 km after that.

Fig. 2.2. Appearance of Osaka Takayasuyama radar (Provided by JMA).

2.5 Operational rawinsonde data

Routine rawinsonde sounding is performing 16 stations by JMA. Fig. 2.3 shows the rawinsonde (RS2-91) to use the JMA. The RS2-91 rawinsonde collects meteorological data such as temperature, humidity, air pressure, wind direction and wind speed in the atmosphere up to 30,000m and transmits it to the ground based data processing system. The data is then automatically processed. The RS2-91 rawinsonde has a built in microprocessor and 4MHz crystal quartz to stabilize the switching signal, reference frequency and pulse band width during a flight allowing for accurate data measurement. The time interval is 12 hours (at 0900, and 2100 JST) at 16 observatories. Specification of the rawinsonde is described in Table 2.1.

Fig. 2.3. RS2-91 type rawinsonde (Provided by Meisei electric Co.,Ltd.).

Table 2.1. Specification of the rawinsonde (RS2-91).

Type	Rawinsonde RS2-91	
Meteorological Sensors	Temperature	Thermister Temperature Sensor
	Range	-85 to 40°C
	Accuracy	± 0.5°C
	Humidity	Capacitive
	Range	5 to 100% RH
	Accuracy	7% on 10–95% RH, 10% on others
	Pressure	Aneroid Capsule (Baroswitch)
	Range	1040 to 5 hPa
	Accuracy	± 1 hPa
Nominal Frequency	1680MHz ±4MHz	
Transmission Power	0.4W at DC15V	
Battery	DC15V water activated battery	
Size	110 × 90 × 180 mm	
Weight	270g including water activated battery	

2.6 Operational wind profiler data

Wind profiler Network and Data Acquisition System (here after WINDAS) is performing at 31 sites by JMA (see Fig. 2.4). The distances from each wind profiler site to its neighboring wind profiler site are ranged from 67 to 262 km, and 130 km on the average over the four main islands of Japan. Particularly, at the south and west coasts of the main islands of Japan, the wind profilers are distributed with higher spatial resolution, so as to correspond to the horizontal scale of meso-β-scale weather systems. The main unit of the wind profilers was designed with the technologies developed at the Radio Science Center for Space and Atmosphere (currently the Research Institute for Sustainable Humanosphere) of Kyoto University (Hashiguchi et al. 2004) in collaboration with the Mitsubishi Electric Corporation. Table 2.2 shows the main characteristics of the WINDAS. The frequency is 1.3 GHz, and the data interval is 10 minutes. Vertical observation range of wind measurement is 6-7 km in summer, 3-4 km in winter, and 5.3 km on the average through at a year. The wind profilers have the transmitting peak power as large as 2 kW, and antenna gain of 33 dBi, by use of 4 m×4 m active phased array antenna, consisting of 96 sub-antennas. A clutter fence, 2 m in height surrounds the array antenna in order to prevent ground clutter contamination. All the wind profilers of the WINDAS are in remote operation from the Control Center, located in Tokyo (Ishihara et al. 2006). We used the data of a wind profiler at Takamatsu station (134.05°E, 34.32°N, 9 m MSL), and Mihama station (135.13°E, 33.89°N, 3 m MSL).

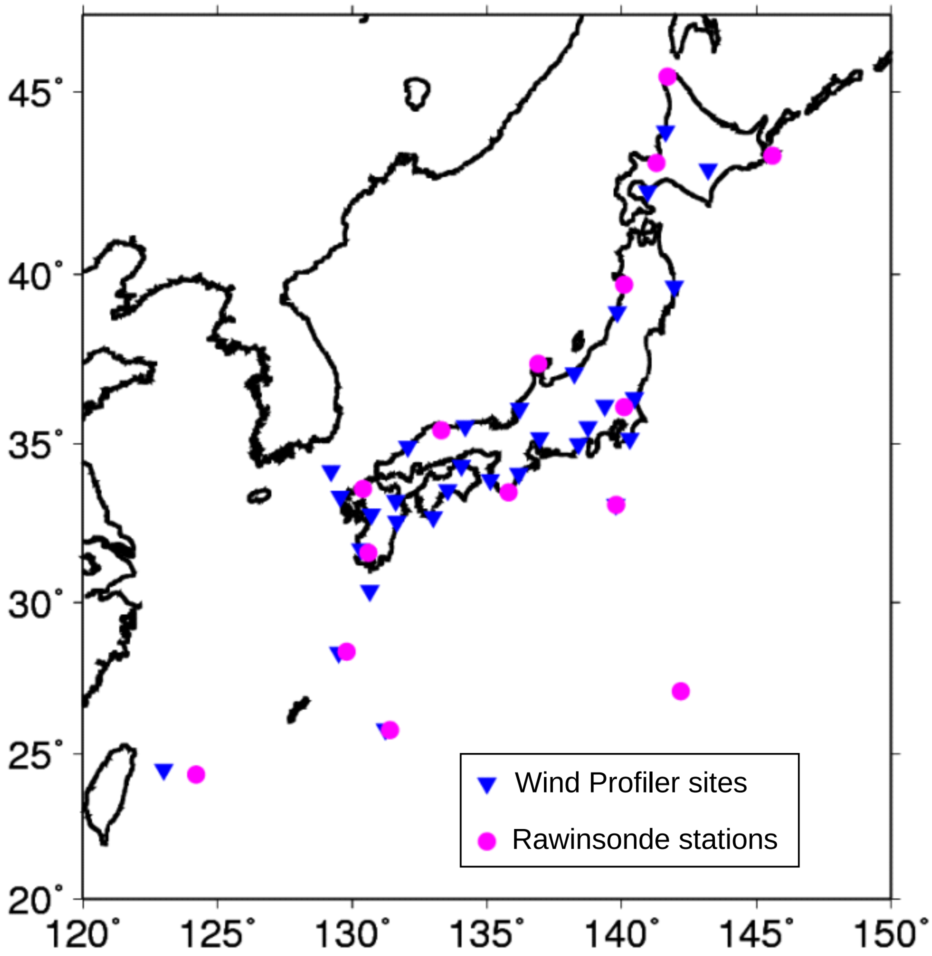

Figure 2.4. WINDAS sites and Rawinsonde stations performed by JMA

Table 2.2. Main characteristics of the WINDAS.

Frequency	1357.5 MHz
Antenna	coaxial colinear arrays with gain of 33 dBi and size of 4 m ×4 m
Peak Power	1.8 kW
Beam width	4 degree
Beam configuration	5 beams
Pulse length	0.67, 1.33, 2.00, 4.00 $\times 10^{-6}$ sec.
PRF	5, 10, 15, 20 kHz
Side robe level	-40 dB or -60 dB at elevation angles of 0–10 degree
Data processing height	400 m to 9.1 km
Vertical resolution	291 m
Basic data	Doppler moments every 1 minute
Distributed data	*u*, *v*, *w*-components of wind, S/N ratio and data quality flag every 10 minutes

2.7 MU radar data

The MU (Middle and Upper atmosphere) radar of the Research Institute for Sustainable Humanosphere (RISH), Kyoto University receives echoes scattered from turbulence and water vapor, and provides vertical profiles of three components including vertical motion of the wind field. The time and height resolutions are 1 min and 150m, respectively.

2.8 Intense rawinsonde observations

We carried out intense rawinsonde observations for two weeks during a Baiu season (26 June-7 July 2006) at two stations: Kobe University (135.24°E, 34.72°N, 145 m MSL) located near the northern coast of Osaka Bay and Shigaraki MU observatory of Kyoto University (136.10°E, 34.85°N, 375 m MSL) located at about 100 km inland from Osaka Bay (see Fig. 2.6). We employed GPS rawinsondes (VAISALA RS-92SGP, see Fig. 2.5) with meteorological balloons (TOTEX TA-200), and obtained vertical profiles of temperature, relative humidity, pressure, and zonal and meridional winds with a time resolution of 2 seconds (corresponding to a vertical resolution of about 5 m s^{-1}). The Vaisala rawinsonde (RS92-SGP) has a reliable code correlating GPS receiver. This receiver has a very fast search engine which ensures that all satellites in view are tracked. Data availability during a sounding is excellent and telemetry errors are always detected. The digital transmitter also consumes less power than an analog transmitter and more channels are available in the meteorological frequency band. Specification of the rawinsonde is described in Table 2.3. In this study, we analyzed mainly the data of rawinsondes launched at 0026, 0257, 0652, and 0932 JST on 2 July at Kobe and at 2334 JST on 5 July at Shigaraki.

Fig. 2.5. RS2-91 type rawinsonde (Provided by Vaisala Co.,Ltd.).

Table 2.3. Specification of the rawinsonde (RS92-SGP)

TEMPERATURE SENSOR TYPE	CAPACITIVE WIRE
Measurement range	-90°C to 60°C
Response time (63.2%, 6 m/s flow)	1000 hPa <0.4 s
	100 hPa <1 s
	10 hPa <2.5 s
Resolution	0.1°C
Accuracy	
Total uncertainty in sounding	0.5°C
Repeatability in calibration	0.15°C
Reproducibility in sounding	1080 - 100 hPa 0.2 °C
	100 - 20 hPa 0.3 °C
	20 - 3 hPa 0.5 °C
HUMIDITY SENSOR TYPE	THIN-FILM CAPACITOR
	HEATED TWIN SENSOR
Measurement range	0 to 100% RH
Resolution	1% RH
Response time	6 m/s, 1000 hPa, +20 °C <0.5 s
	6 m/s, 1000 hPa, -40 °C < 20 s
Accuracy	
Total uncertainty in sounding	5% RH
Repeatability in calibration	2% RH
Reproducibility in sounding	2% RH
PRESSURE SENSOR TYPE	SILICON
Measurement range	1080 hPa to 3 hPa
Resolution	0.1 hPa
Accuracy	
Total uncertainty in sounding	1080 - 100 hPa 1 hPa
	100 - 3 hPa 0.6 hPa
Repeatability in calibration	1080 - 100 hPa 0.4 hPa
	100 - 3 hPa 0.3 hPa
Reproducibility in sounding	1080 - 100 hPa 0.5 hPa
	100 - 3 hPa 0.3 hPa
DIMENSIONS AND WEIGHT	Dimensions 220 x 80 x 75 mm
Weight with water-activated battery	(RS92-SGPW) Typically 250 g 1
WATER-ACTIVATED BATTERY (ORDER CODE RS92-SGPW)	Voltage 8V, nominal

Operating time	135 min
TELEMETRY	
Transmitter type	Synthesized
Frequency band	403 MHz
Tuning range	400 - 406 MHz
Frequency stability	90 % probability ± 2 kHz
Deviation, peak-to-peak	4.8 kHz
Emission bandwidth	According to EN 302 054
Output power (high-power mode)	60 mW min
Modulation	GFSK
Data downlink	2400 bit/s, digital
Measurement cycle	1 s

2.9 Mesoscale model

A mesoscale numerical model called MM5V3 developed by Pennsylvania State University (PSU) and US National Center for Atmospheric Research (NCAR) (Grell et al. 1994) was used for complementing observations. The MM5 is a nonhydrostatic model, and is composed by two domains with a two-way nesting: Domains 1 and 2 with horizontal resolutions of 6 and 2 km, respectively.

In this study, the cloud and precipitation process was represented by the Reisner micro-physical parameterization (Reisner et al. 1998), which predicts the mixing ratio of cloud water and ice crystals, as well as rain, graupel, and snow water mixing ratios. Turbulent fluxes in the planetary boundary layer were parameterized utilizing a scheme used in the NCEP medium-range forecasting (MRF) model (Hong and Pan 1996). Radiative processes in the free atmosphere were parameterized using a scheme incorporating effects due to modeled clouds. The Kain-Fritsch cumulus parameterization (Kain and Fritsch, 1990) was used in Domain 1, to determine updraft/downdraft properties and detrainment between cloud and precipitation in addition to vapor. The initialized time was 0300 JST for 9-h forecast for the first day and the initialized time was 1500 JST for 9-h forecast for the last day. The MANAL data are applied to provide the initial and boundary conditions, respectively for the model atmosphere. Daily sea surface temperatures are obtained from the National Centers for Environmental Prediction (NCEP). These data are interpolated to the MM5 model grid using the standard preprocessing programs provided by NCAR. Domain 1 (see Fig. 2.6) consisted of 151 grid points, and Domain 2 with 181 grid points is centered at 34.0°N, 134.0°E. 48 unevenly spaced sigma levels are used, of which the finest resolution is located near the surface. The model top is set at a constant pressure of 100-hPa level. 2′- and 30″- averaged terrain, vegetation/land-use, and land-water mask datasets produced by US Geological Survey were used for Domain 1 and 2, respectively.

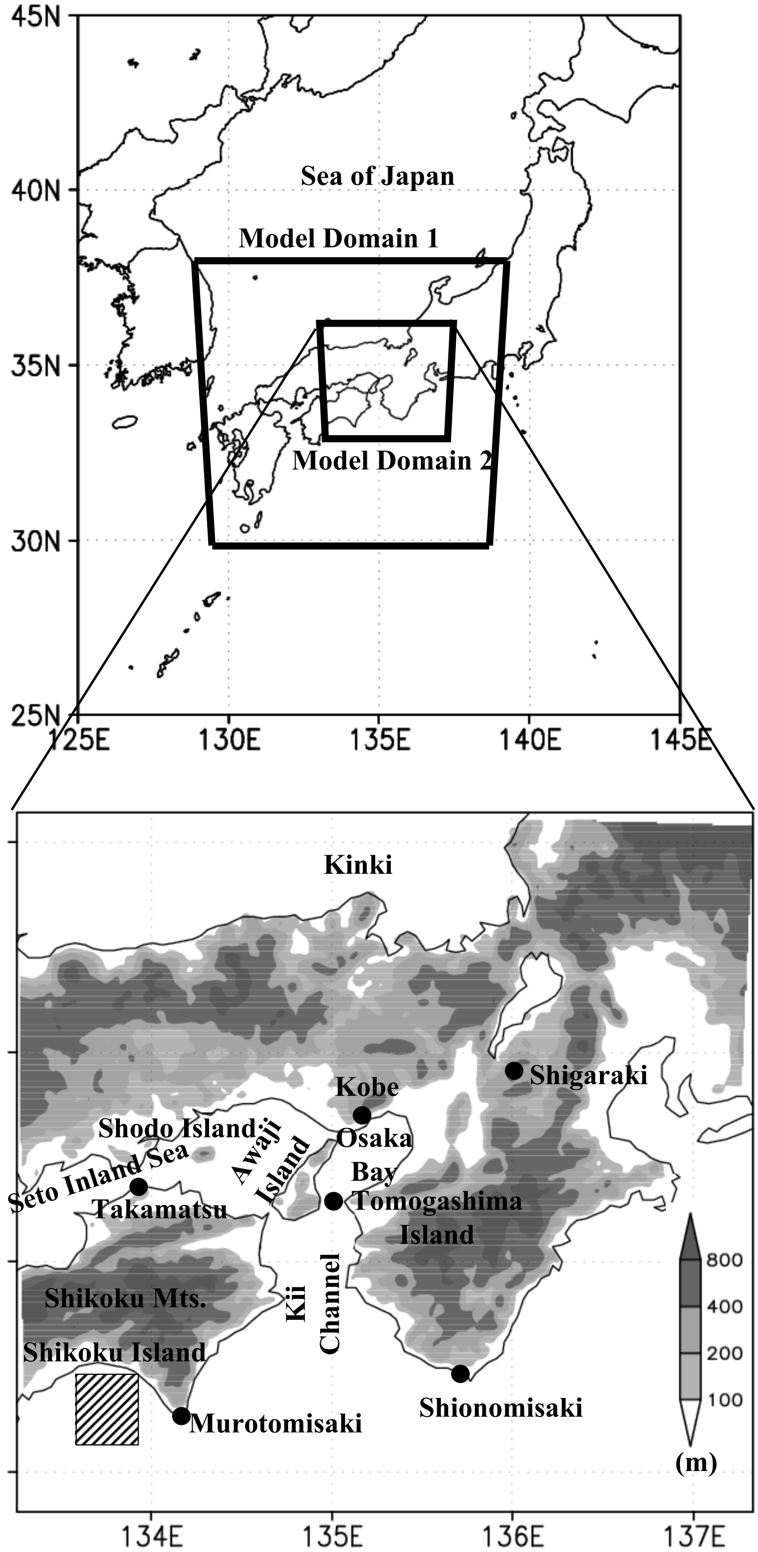

Figure 2.6. Maps of Japan Islands (upper) and around Kinki district (bottom). Shade indicates the topography. Model domains 1 and 2 used in Section 3 are also shown. The hatched square indicates the area used in investigating wind field based on MANAL 16 grid data.

Chapter 3

Climatological analysis

3.1 Analysis method

We used the JMA Osaka Takayasuyama radar data (see Section 2.4) to investigate whether formed the line-shaped precipitation band or not in 1999. The line-shaped precipitation band was defined that the rainfall intensity derived from the radar echo was over 16 mm h^{-1} and the echo existed from southwest to northeast around Osaka Bay. We studied passage of the cold front around Osaka Bay in 1998–2007 using the JMA weather maps. The cold front is defined as maxima of horizontal temperature gradient and vertical component of vorticity near the surface, and temperature inversion layer representing the frontal surface (Ogura and Portis 1982). The cold front position is determined every one hour by linear interpolated because the surface weather maps is provided four times per day (0300, 0900, 1500, 2100 JST). The three-hourly accumulated precipitation maps were made by Radar-AMeDAS data and we investigated how much precipitation by the cold front. Next the climatologically estimated appearance rate and precipitation intensity are classified by the wind direction, because the low level southerly carry the moist and warm air to need formation and maintenance the line-shaped precipitation band. In Osaka Bay, the southerly easily approach in Kii Channel, and Tomogashima weather station is good location to investigate the low level wind field. We used the surface weather data described in Section 2.3.

3.2 Results for 1999

Cold fronts passed 22 times over Osaka Bay in this period in 1999. The passages were frequent in January (1 time), February (2 times), March (1 time), April (4 times), May (3 times), June (3 times), from July to August (1 time), November (3 times) and December (1 time). Among them, three cases accompanied line-shaped precipitation system with heavy rainfall, and the other 19 cases did not. The three line-shaped precipitation systems brought heavy rainfall (over 100mm/3 hours) in Kinki District (May 27, Jun 27, Jun 29, see Fig. 2.1). Based on the upper air sounding over the Shionomisaki weather Station, southwesterly winds over 20 m s^{-1} were dominated in lower layer in these three heavy rainfall cases.

Based on this climatological feature, we made detailed analysis for 1999. The three line-shaped precipitation systems brought heavy rainfall (May 27, Jun 27 and Jun 29). At May 27, 925-hPa level wind direction is southwesterly, and wind speed is 27.5 m s^{-1} in Table 3.1. At Jun 27 and 29, 925-hPa level wind directions are also southwesterly, and wind speed is over 20 m s^{-1}.

Especially, at Jun 27 and 29, the convective available potential energy is over 1000 J kg^{-1}. Strong southwesterly wind with 20 m s^{-1} is dominant, and existed unstable layer in the heavy rainfall cases.

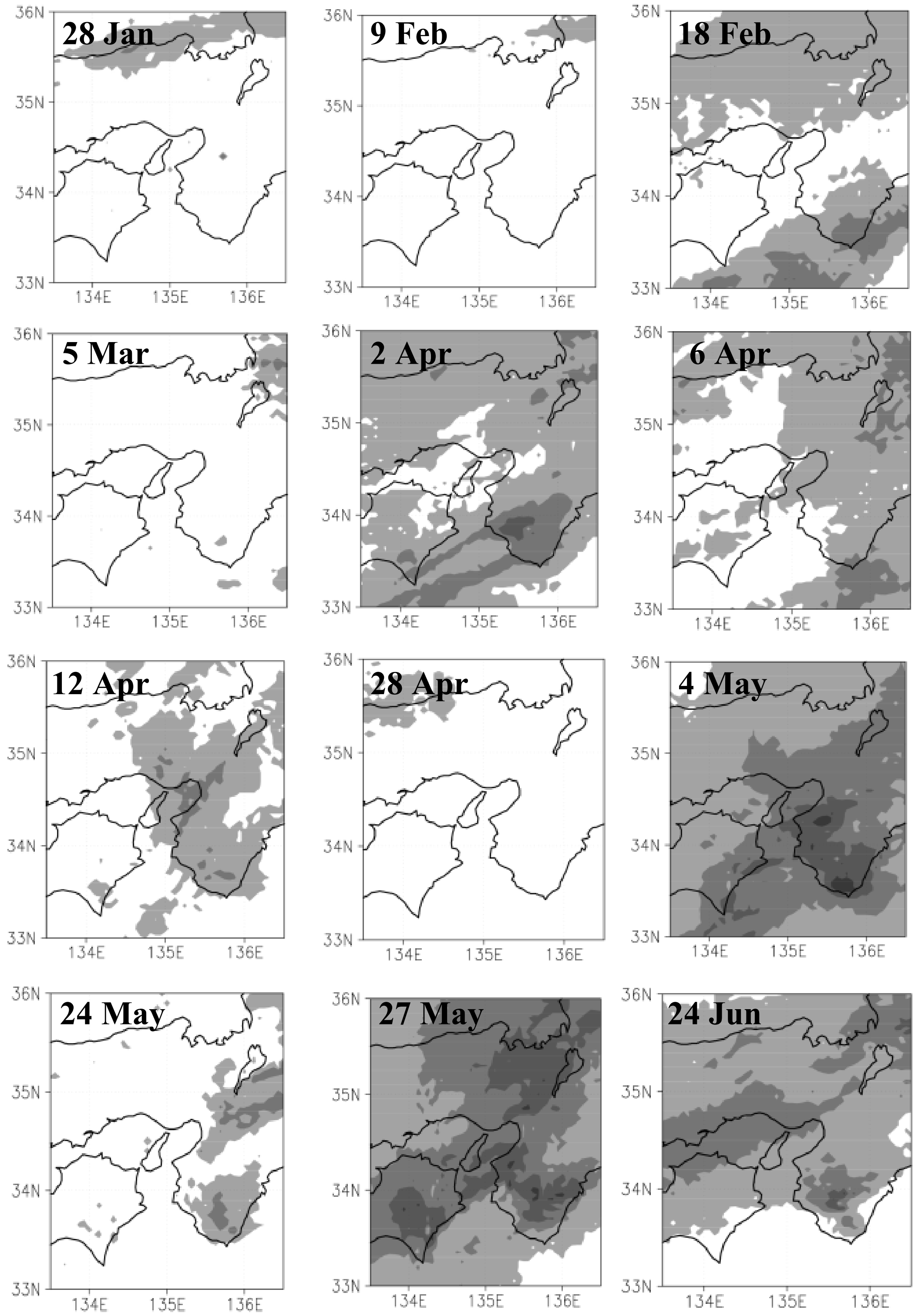

Figure 3.1. Horizontal distributions of precipitation echo intensity at 2 km height level observed by the JMA operational radars in 1999.

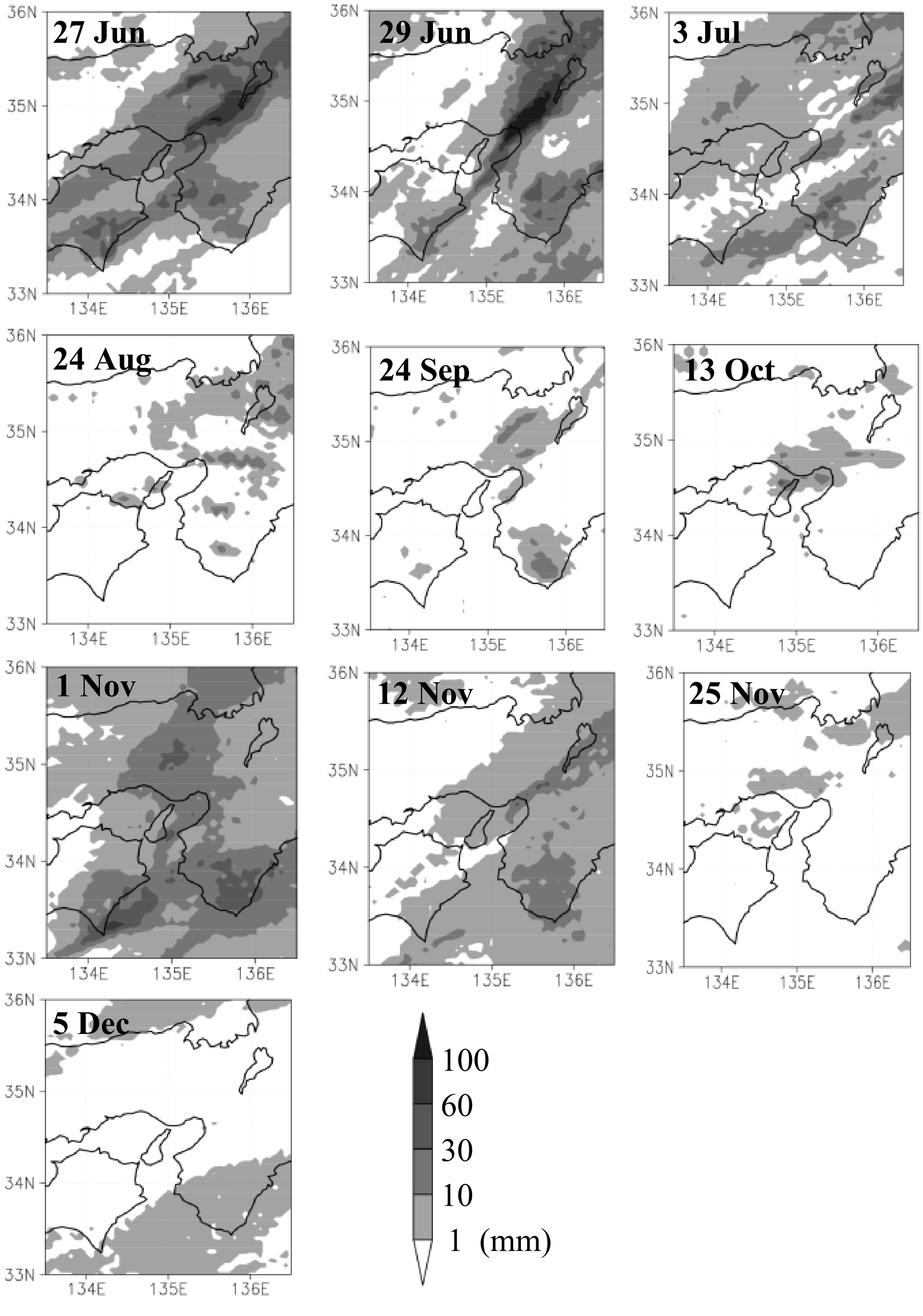

Continued Fig. 3.1

Table 3.1. Cases of passage of cold front around Osaka Bay in 1999. Symbol ○ is indicated by organized line-shaped precipitation band (including the precipitation intensity ≥ 100 mm in three hours). Wind direction and speed is indicated at 925-hPa level, and convective available potential energy is presented by Shionomisaki rawinsonde observational station.

Day Month	Line-shaped precipitation band	Wind Direction 925 hPa (deg)	Wind Speed 925 hPa ($m\ s^{-1}$)	Convective available potential energy ($J\ kg^{-1}$)
28 Jan		305	16.7	0
9 Feb		265	10.3	0
18 Feb		235	12.4	9
5 Mar		190	6.5	0
2 Apr		230	13.5	25
6 Apr		200	8.6	27
13 Apr		190	8.6	22
28 Apr		300	8.6	0
4 May		175	13.5	92
24 May		240	23.2	381
27 May		230	27.5	379
24 Jun		250	25.4	415
27 Jun	○	230	21.1	1123
29 Jun	○	215	23.2	1787
3 Jul		240	18.9	822
24 Aug		290	8.6	1480
24 Sep		180	20.0	1376
13 Oct		270	8.6	712
1 Nov		220	29.2	3
12 Nov		175	14.6	393
25 Nov		275	9.2	0
6 Dec		260	8.6	0

3.3 Characteristic features of the line-shaped precipitation bands

The line-shaped precipitation band is defined by a line-shaped precipitation area lying in a southwest to northeast direction that meteorological radar observed including for larger 30 mm h^{-1} around Osaka Bay. We have examined all the data similar to Fig. 3.1 during 2003-2007 (see Table 3.2 and Fig. 3.2). Cold fronts passed 99 times over Osaka Bay in this period. The passages were frequent in March (11 times), April (14 times), May (13 times) and July (15 times), but less than 6 times in January, February, August, October and November. This feature has been found in a similar preliminary study for 1999. Based on this climatological feature, we made detailed analysis for July from 2003 to 2007. Among the 15 cases in July, we found four cases (Cases K, L, M and N) with the meso-β-scale lows and pressure troughs in around the eastern part of Shikoku Island. When the meso-β-scale low was formed wind in around Shikoku is relatively stronger than the other cases.

Table 3.2. A list of cold fronts passed around Osaka Bay in July from 2003 to 2007. Wind speed is one day averaged wind in Murotomisaki weather station (185m MSL). The cases in which the meso-β-scale low and line-shaped precipitation band were detected denoted by the symbols of O.

	Year	Day	Time (JST)	Wind speed (m s^{-1})	Meso-β-scale low	Line-shaped precipitation band (Echo intensity over 30 mm h^{-1})
A	2003	3	21	9.3		
B	2003	7	15	8.7		
C	2003	12	3	8.7		
D	2003	21	9	5.3		
E	2003	24	3	4.5		
F	2003	30	9	6.7		
G	2004	5	9	8.4		
H	2004	10	15	5.4		
I	2005	4	21	8.6		
J	2005	10	21	10.0		
K	2005	12	9	9.4	○	
L	2006	2	9	15.8	○	○
M	2006	5	21	17.3	○	○
N	2006	21	9	14.0	○	
O	2007	11	12	4.6		

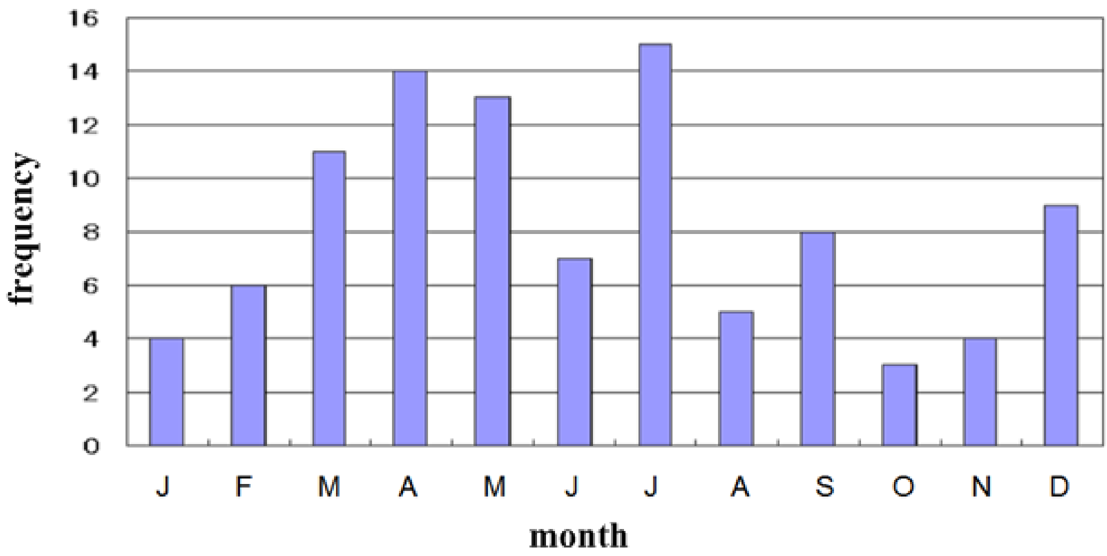

Figure 3.2. Histogram of cold front passages during 2003–2007.

3.4 Averaged appearance rate and precipitation intensity classified by the wind direction and speed

Appearance rate distributions of precipitation are classified by wind, observed by Tomogashima surface weather station in Fig. 3.3. The distribution of all data shows that appearance rate increase around mountain region. It should be noted that total appearance rate of northwesterly and southerly wind fields is larger the other wind directions. Since these previous studies are pointed out important to southerly or southwesterly wind to form the line-shaped precipitation band, we focus the southerly. Appearance rate is 14.0 %. In the distribution of the S, the peak of precipitation is appeared to northeast direction from Osaka Bay, but the other peak does not appear. Therefore the southerly inflow is important role of formed the line-shaped precipitation band.

The distributions of averaged precipitation intensity classified by wind direction, observed Tomogashima, are shown in Fig. 3.4. The distribution of all data shows that strong rainfall areas are not found around the Osaka Bay. The southerly, south-southwesterly, and southwesterly wind field, the precipitation intensity is larger than the other wind directions. Fig. 3.5 shows that the line-shaped precipitation bands are not found when low level winds are weak (< 10 m s^{-1}). At 10~15 m s^{-1}, a weak band like precipitation area appears northeastern of Osaka Bay, but this is not remarkable. The line-shaped precipitation peak is gradually remarkable at 15~20 m s^{-1}, especially, at 20~25 m s^{-1} the band like precipitation peak is clearly around northeastern side of Osaka Bay.

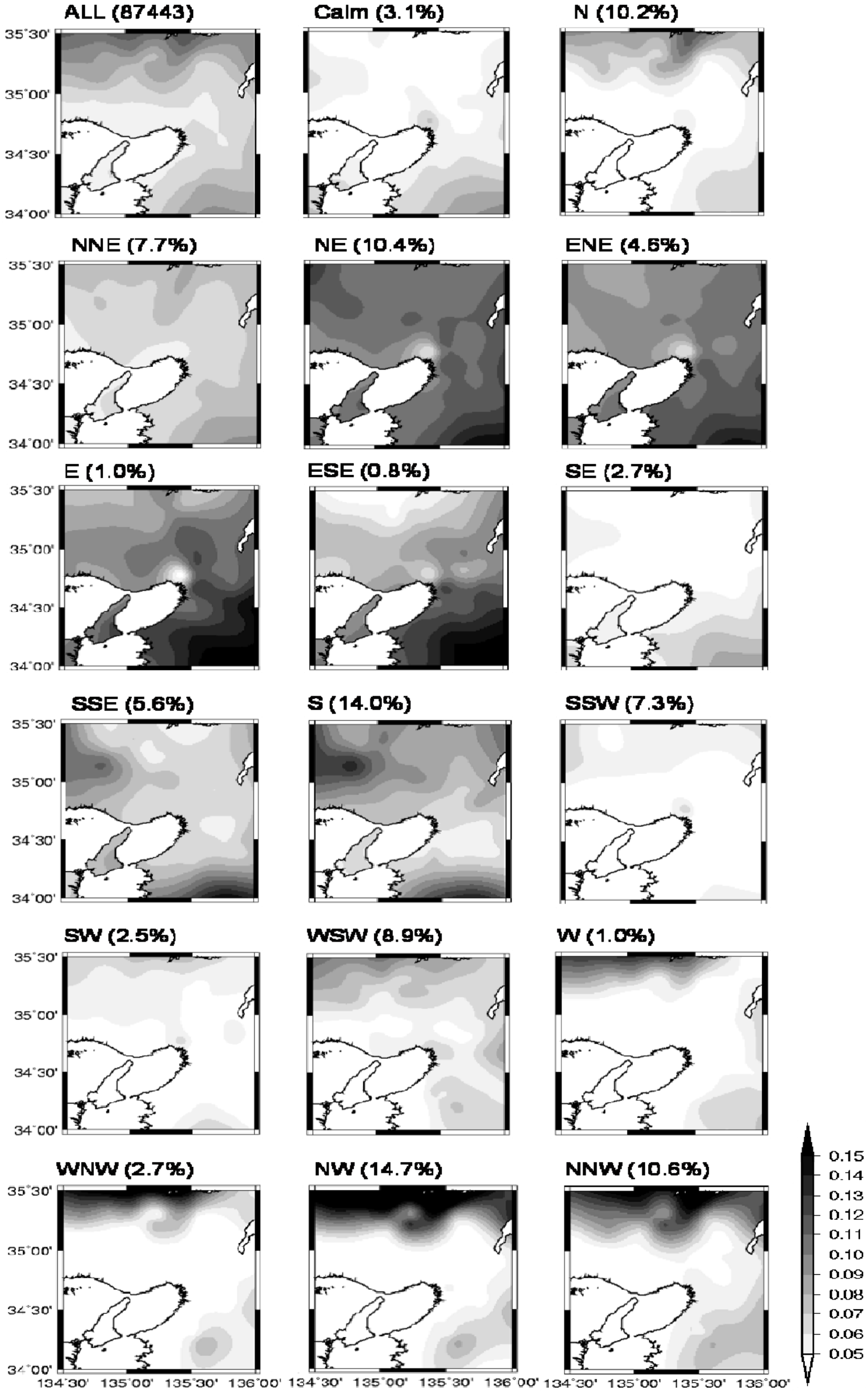

Figure 3.3. Appearance rate distributions of precipitation classified by wind direction, observed by surface weather station at Tomogashima. These rates were averaged during 1500JST 31 Mar 1998 and 1400JST 31 Mar 2008. Appearance rates of each wind direction are shown in the parenthesis (%), but observation total number is shown in all.

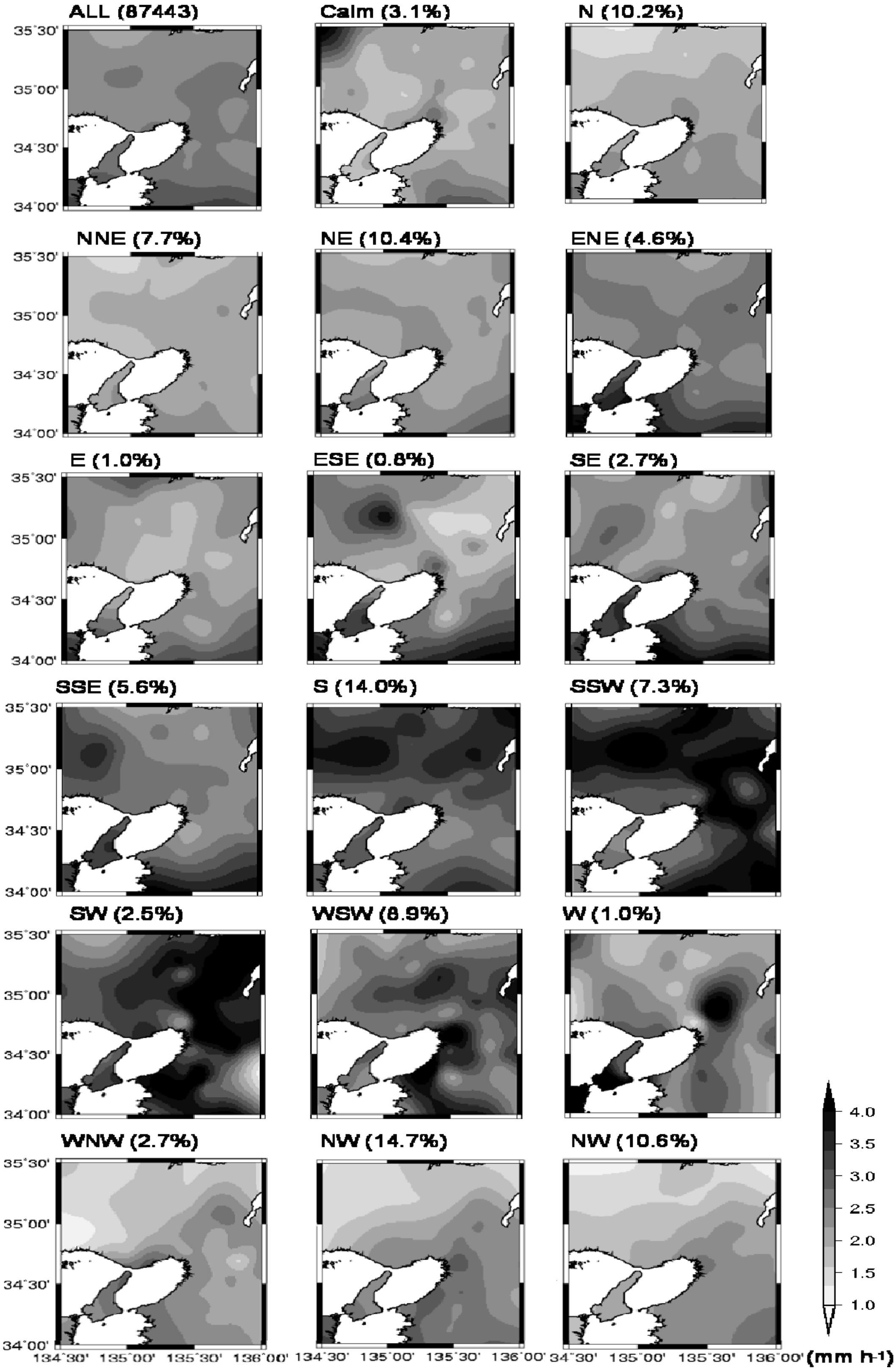

Figure 3.4. Same as Fig. 3.3, but for precipitation intensity (mm h^{-1}).

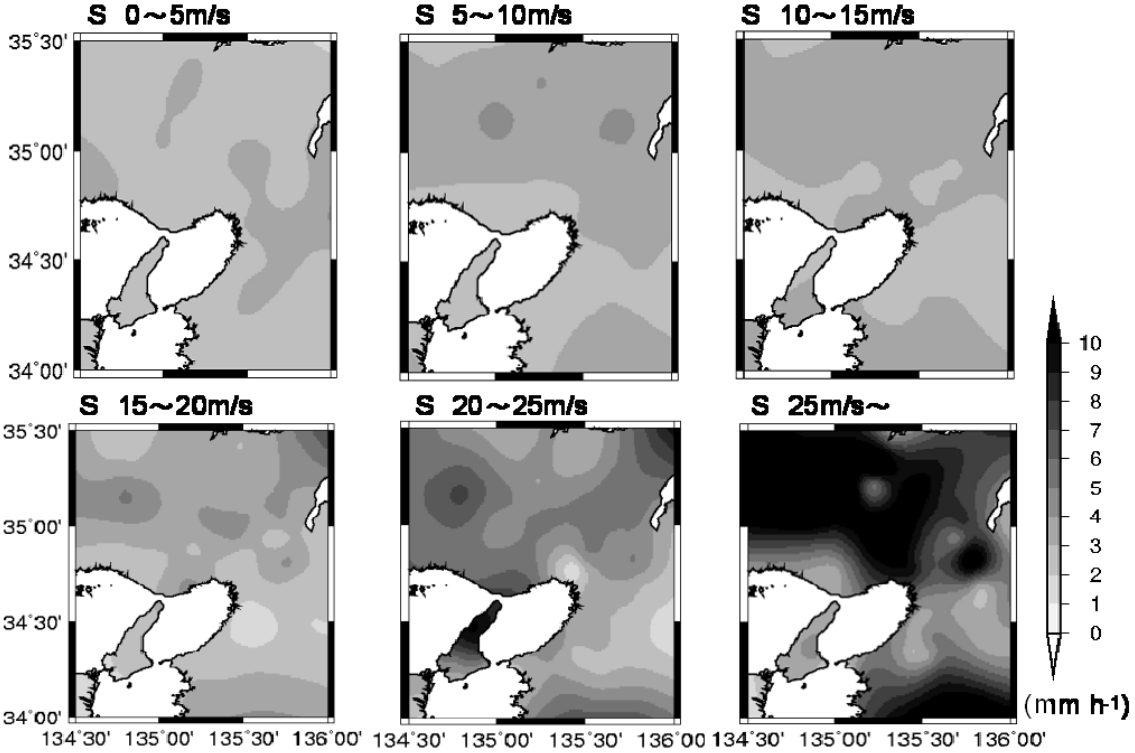

Figure 3.5. Same as the S case in Fig. 3.4, but for classified each wind speed (every 5 m s^{-1}).

3.5 Discussions

Some case studies indicated that when the line-shaped precipitation band appears around Osaka Bay, the strong southerly (at least 10 m s^{-1}) is dominant around Kii Channel (Yokota 1993; Higashi and Fujii 2004). In 1999, when the line-shaped precipitation band appears around Osaka Bay, the 925-hPa level wind speed is more than 20 m s^{-1} at Shionomisaki. Therefore we consider that the southerly is important condition to form the line-shaped precipitation band around Osaka Bay. The similar features are seen to some case studies of Kyusyu area. For example, Kato (2003) pointed out that the intense southerly or southwesterly from tropics in the lower layer with a height of about 1 km is necessity to form the Koshikijima and Nagasaki lines.

The favorable conditions for their formation and maintenance were that the southwesterly low -level wind field persists for longer than 12 hours, and that the wind speed at an 850-hPa level is between 5–25 m s^{-1} (Kato 2005). In our results, when the wind direction is southerly, the line-shaped precipitation band is formed easily for the other wind directions. When the southerly is less than 10 m s^{-1}, the band like precipitation peak is not seen to around Osaka Bay, but as the southerly more than 10 m s^{-1}, gradually we appear the band like structure. These results are consistent with previous case studies. The band like precipitation peak is distinguished, when the southerly is between 20–25 m s^{-1}. Therefore, we consider that the strong southerly (about 20 m s^{-1}) is one of the conditions of formed the intense line-shaped precipitation band around Osaka Bay.

Chapter 4

Case studies

4.1 Case studies in 1998 and in 2003

In this section two case studies on line-shaped precipitation bands appeared in October 1998 and April 2003 are briefly distributed. These not in Baiu season, but environmental conditions were some features similar to late Baiu season which will be described in detail in the next subsection.

4.1.1 Background field generating the line-shaped precipitation bands

Figures 4.1 and fig. 4.2 show distributions of precipitation intensity on 15 Oct 1998 from 1800 to 2200 JST and on 8 Apr 2003 from 1000 and 1400 JST, respectively. At 15 Oct, the small radar echo appeared around Mt. Rokko at 1800 JST. At 1900 JST, the echo was strong ($\geq$ 30 mm h^{-1}) in same area and the echo was gradually line-shaped. The echo extended to northeast, and arrived in Kyoto area at 2000 JST. At 2100 JST, the echo more extended to northeast, however the line-shaped precipitation band was almost stagnant until 2400 JST. The around line-shaped precipitation area was not appear the other rainfall systems. The three hourly accumulated rainfalls from 2000 to 2300 JST of 139.5 mm, and a maximum hourly accumulated rainfall of 73.5 mm were observed at Kyoto Meteorological Observatory (KMO). This hourly accumulated rainfall amount was fifth on record from Jan 1906 to Aug 2003. In Kyoto Sangyo University (KSU) which is located 7km north-northeast from KMO, the three hourly accumulated rainfalls from 2000 to 2300 JST of 125.0 mm, and a maximum hourly accumulated rainfall of 69.0 mm were observed by own rain gauge. However the three hourly accumulated rainfalls of only 15.5 mm was observed in Hanasetouge which is AMeDAS site located 10 km north from KSU. The other AMeDAS site around Kyoto city (Nagaokakyo, Sonobe, Keihoku and Kyotanabe) was hardly precipitation (less than 3mm h^{-1}).

At 8 Apr, the rainfall systems approached Kinki District at 1000 JST, but this system was not line-shaped. After 1100 JST, the rainfall systems were gradually line-shaped and this is stagnant on Osaka Bay until 1300 JST. After 1300 JST, the line-shaped precipitation band was disappeared and moving eastward gradually. A maximum hourly accumulated rainfall of 34.0 mm h^{-1} was observed from 1100 to 1200 JST at Ashiya AMeDAS site. In Rokko elementally school, a maximum hourly accumulated rainfall of 60.0 mm h^{-1} was observed by rain gauge of installed Atmospheric Hydrostatic Science Laboratory in Kobe University.

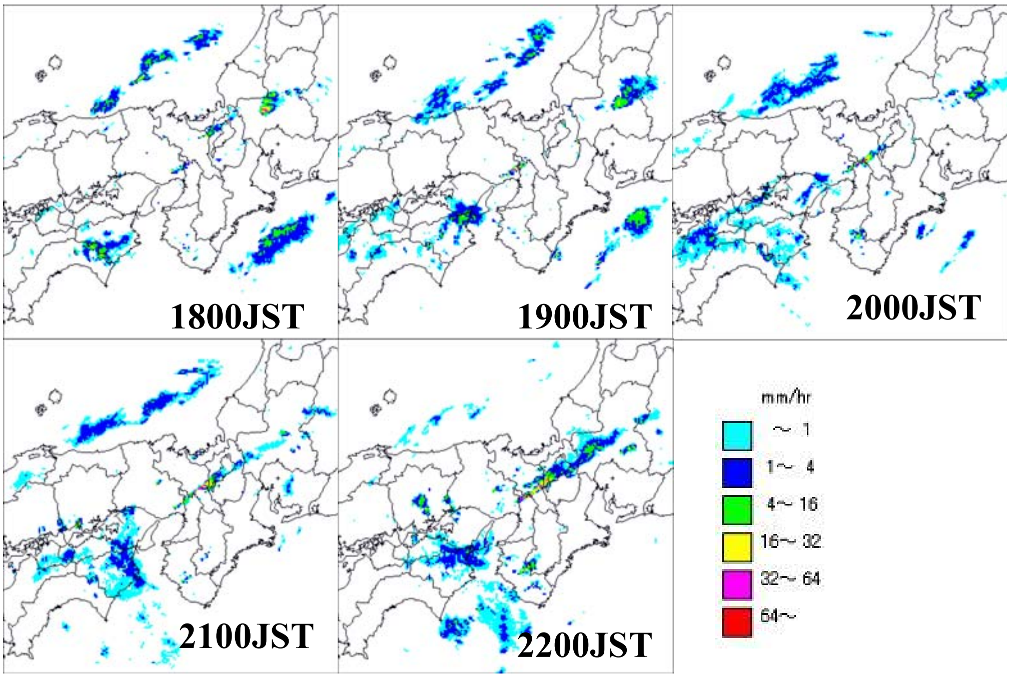

Figure 4.1. Horizontal distributions of precipitation echo intensity at 2 km height level observed by the JMA operational radars from 1800 to 2200 JST on 15 Oct 1998.

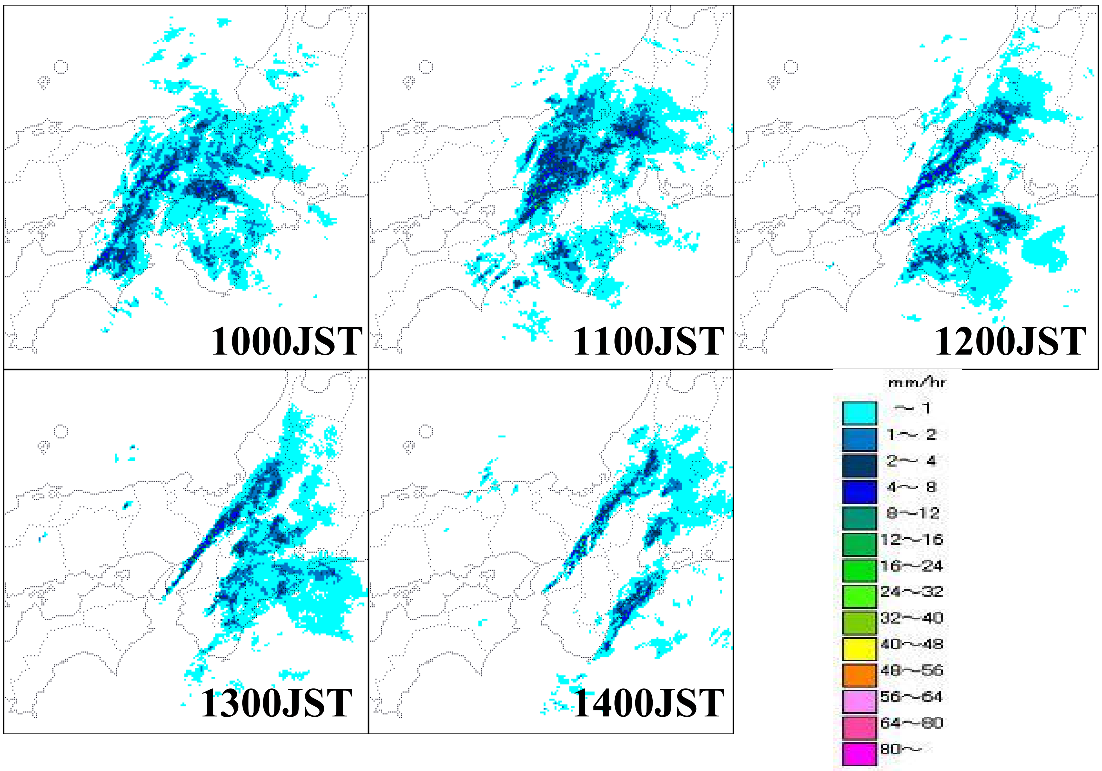

Figure 4.2. Horizontal distributions of precipitation echo intensity at 2 km height level observed by the JMA operational radars from 1000 to 1400 JST on 8 Apr 2003.

Figure 4.3 shows surface, 850-, and 500-hPa levels weather maps at 2100 JST on 15 Oct 1998. At surface level, a cyclone is seen to north of Hokkaido. The central pressure of cyclone which accompanied by occluded front is 992 hPa. A occluded front extending from 50°N, 150°E, the cold front extended from occluded point to Kinki District. A typhoon 10 (T10) also appear around Taiwan Island. At 850-hPa level, the humid area (T–Td ≤ 3 °C) expanded west Japan from tropic oceans around T10. At 500-hPa level, the horizontal wind was easily to tropic oceans because a pacific high is located southeast pacific ocean.

Figure 4.3 also weather maps on 8 Apr 2003. At surface level, a cyclone is seen over Sea of Japan. The central pressure of cyclone which accompanied by cold front is 998 hPa. A cold front extended from located over the Kinki District. At 850-hPa level, the low pressure corresponded to surface cyclone existed, the short-wave trough existed along 130°E. Kinki District is located on the ridge and the warm air was covered in this area.

Figures 4.4 shows vertical profiles of humid number (T–Td) and equivalent potential temperature (θ_e) observed at 2100 JST on 15 Oct 1998, and 0900 on 8 Apr 2003, from Shionomisaki weather station. In 1998, the θ_e decreased from surface to 5 km altitude and the dry air existed between 4 and 6 km altitude. Such condition is convective instability which increases as the upper-level atmosphere becomes dry. The LCL is 957-hPa level and the LFC is 922-hPa level. Therefore if it lifts the air parcel a little, the air is condensed easily.

In 2003, the θ_e decreased from surface to 2 km altitude and the dry air existed over 5 km altitude. It also appeared to convective instability in this case. The LCL is 948-hPa level and the LFC is 936-hPa level. In this case, we can investigate θ_e horizontal field of each height, since we can use MANAL data. The 500-hPa level and 950-hPa level equivalent potential temperature (θ_e) fields, the surface wind and sea level pressure depicted from the MANAL at 0900 JST on 8 Apr are shown in Fig. 4.5. A meso-β-scale low is found in the east of Shikoku Island (134.3°E, 33.7°N) and Kii peninsula (135.6°E, 34.2°N). A strong southwesterly wind flows to east of the lows. It merges with strong south wind (≥ 10 m s^{-1}) region with high θ_e (>320 K) area at the 950-hPa level. The relatively high θ_e area is like a "moist tongue". At 500-hPa level, the southwesterly wind with a speed of about 20 m s^{-1} is dominant. A relatively low θ_e (<315 K) area approached from west of Kinki District.

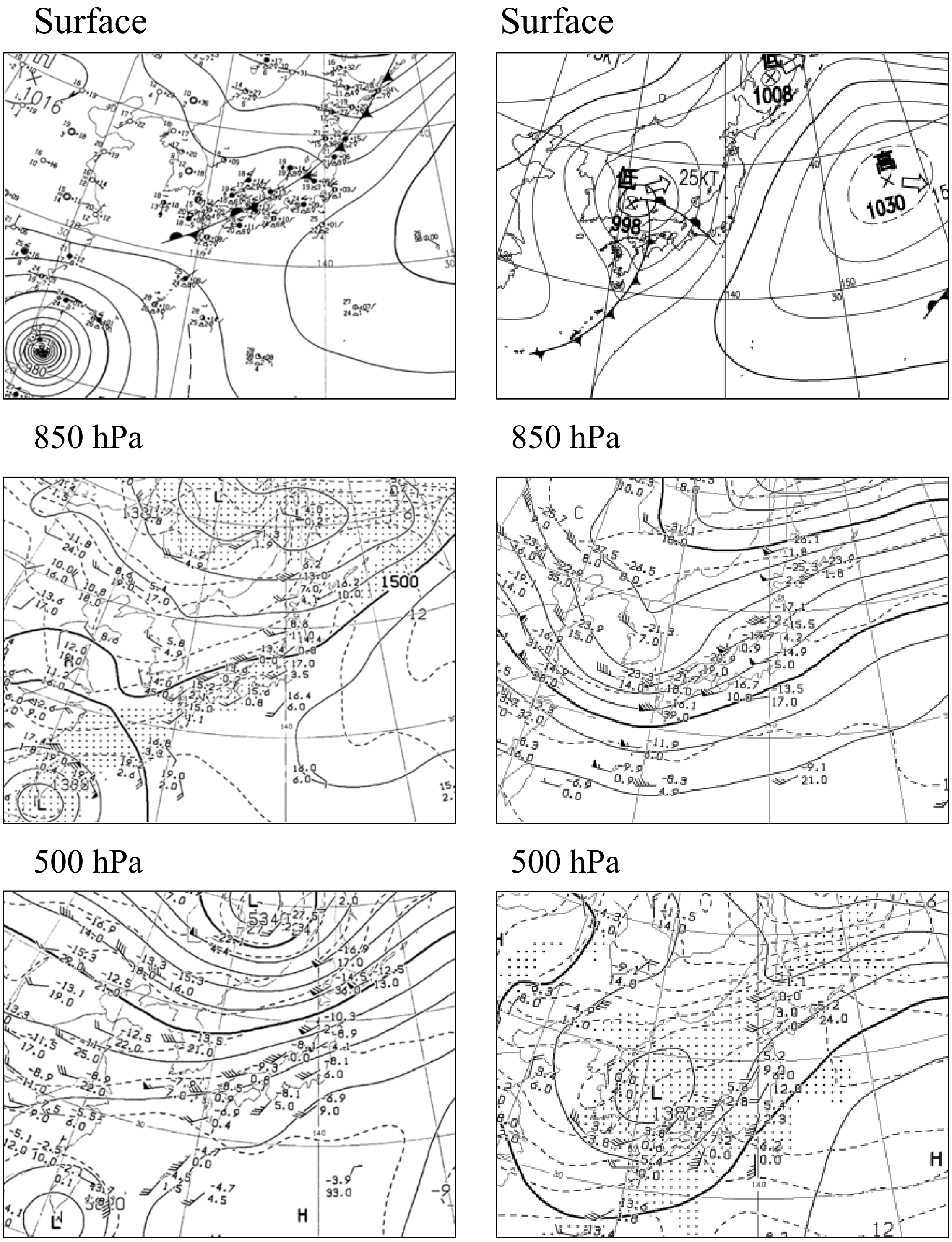

Figure4.3. Weather maps of surface, and 850- and 500-hPa-levels at 2100 JST on 15 Oct (left-hand side panels) and 0900 JST on 8 July (right-hand side panels). In the 850- and 500-hPa levels weather maps, solid and dashed lines indicate geopotential height (m) and temperature (°C). In 850-hPa level, the dotted area is wet area ($T - T_d \leq 3$ °C).

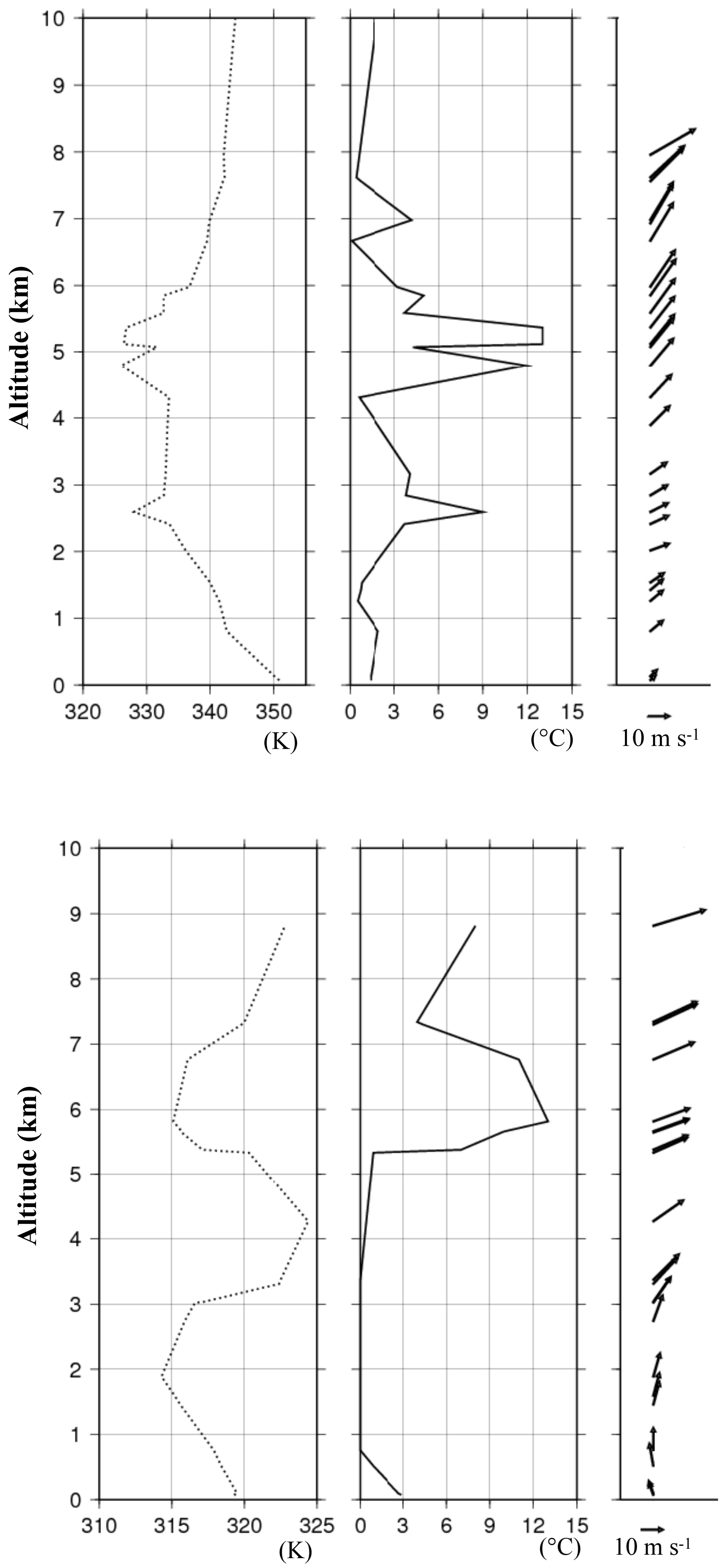

Figure 4.4. Vertical profiles of equivalent potential temperature (dashed line), humidity number ($T–T_d$, solid line), and wind vector observed at 2100 JST on 15 Oct (upper panel), and 0900 JST on 8 Apr (lower panel).

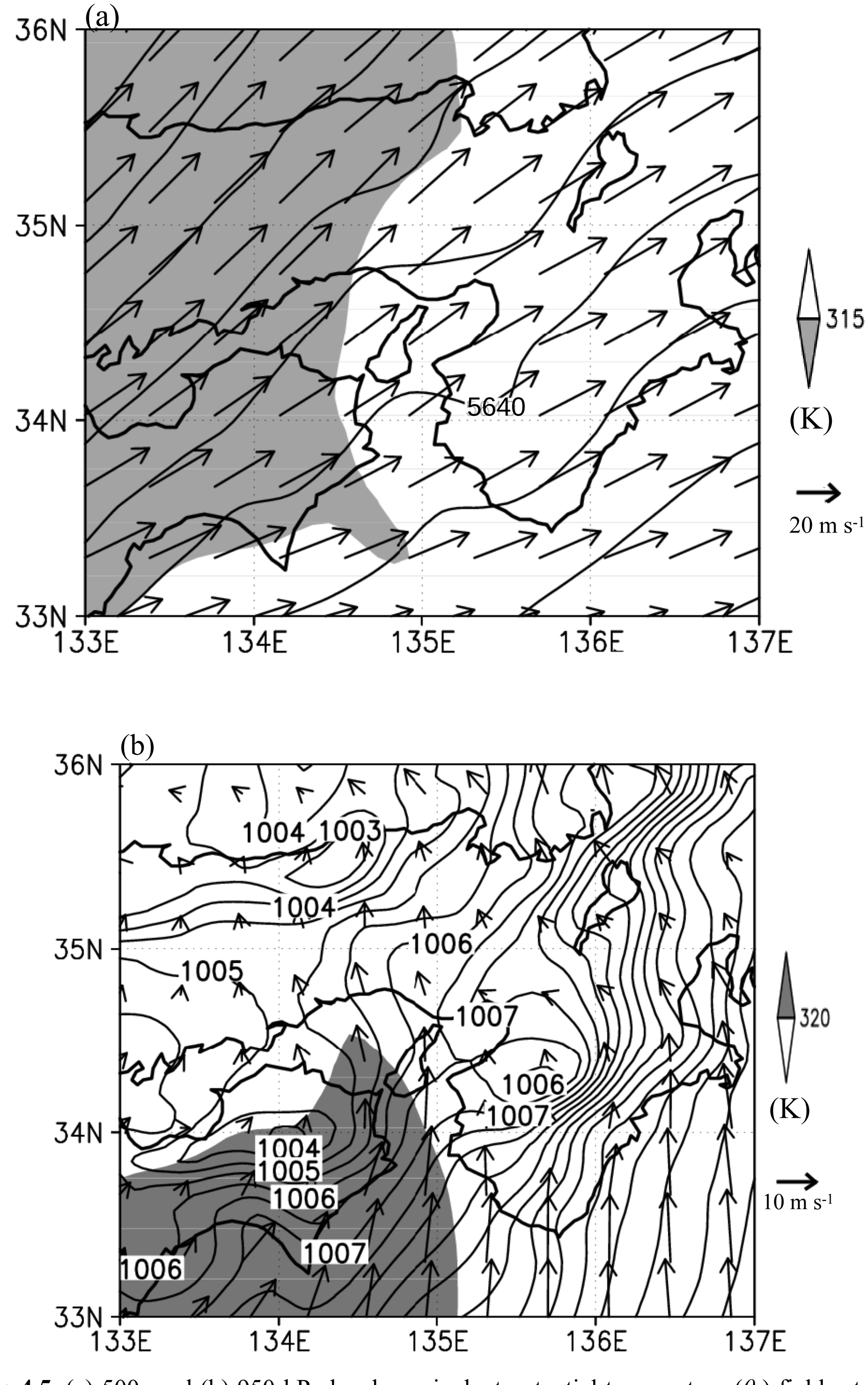

Figure 4.5. (a) 500- and (b) 950-hPa levels equivalent potential temperature (θ_e) fields at 0900 JST on 8 Apr. Contours show (a) geopotential height (m) and (b) sea level pressure (hPa). Arrows indicate (a) 500 hPa and (b) surface wind (m s^{-1}).

4.1.2 Wind behavior near the line-shaped precipitation bands

In 1998, we used only AMeDAS data to investigated wind filed around precipitation band, since wind profiler system was not installed and MANAL data did not existed. Table 4.1 shows the wind direction and speed at Tomogashima and Ieshima AMeDAS site during 1800 to 2400 JST. The south wind was continued flowing and the wind speed about 10 m s^{-1} in the period. In Ieshima, the wind speed was less than 2 ms^{-1} in the period. Therefore the south wind was dominant around Kii Channel, but the westerly wind did not existed around Seto Inland sea.

In 2003, at 950-hPa level at 0900 JST on 8 Apr, a meso-β-scale low existed to east of Shikoku Island and Kii Peninsula (see Fig. 4.5). The south wind was dominant around the surface and the wind speed was about 20 m s^{-1} around the eastern side of Shikoku meso-β-scale low. On the other hand, the southeasterly wind appears to north and northeast side of the Kii Peninsula meso-β-scale low. Figure 4.6 shows Takamatsu and Wakayama Mihama wind profiler data. The south wind was dominant in Mihama below 2 km altitudes, however the wind direction is gradually clockwise rotated as with the altitude, the southwesterly wind was dominant over 2 km altitudes during 0900 to 1200 JST. The westerly wind was dominant around Seto Inland Sea below 1 km from 0930 JST at Takamatsu. Figure 4.7 shows zonal wind component at Shigaraki MU radar site from 0300 to 1200 JST. The east wind component appeared to below 2 km altitude until 1400 JST. Especially relatively strong east wind component (between 3.5 and 5 ms^{-1}) was dominant from 0500 to 1200 JST. In this period, a meso-β-scale low existed in Kii Peninsula. The east wind component was related to the meso-β-scale low, because MU radar site is located north-northeast from the meso-β-scale low.

Table 4.1. Wind direction and speed during 1800 and 2400 JST on 15 Oct, from Tomogashima and Ieshima AMeDAS stations. "-" indicates calm wind.

time	Tomogashima wind		Ieshima Wind	
	direction	speed	direction	Speed
(JST)	(deg.)	(m s^{-1})	(deg.)	(m s^{-1})
1800	180	8	202.5	2
1820	180	8	180	1
1840	180	8	157.5	1
1900	180	10	180	2
1920	180	10	180	2
1940	180	10	202.5	1
2000	180	10	0	2
2020	180	9	337.5	2
2040	180	9	-	0
2100	180	10	292.5	2
2120	180	11	315	1
2140	180	9	337.5	2
2200	180	8	337.5	1
2220	180	10	337.5	1
2240	180	9	270	1
2300	180	8	225	1
2320	180	7	247.5	2
2340	180	7	270	2
2400	180	7	270	1

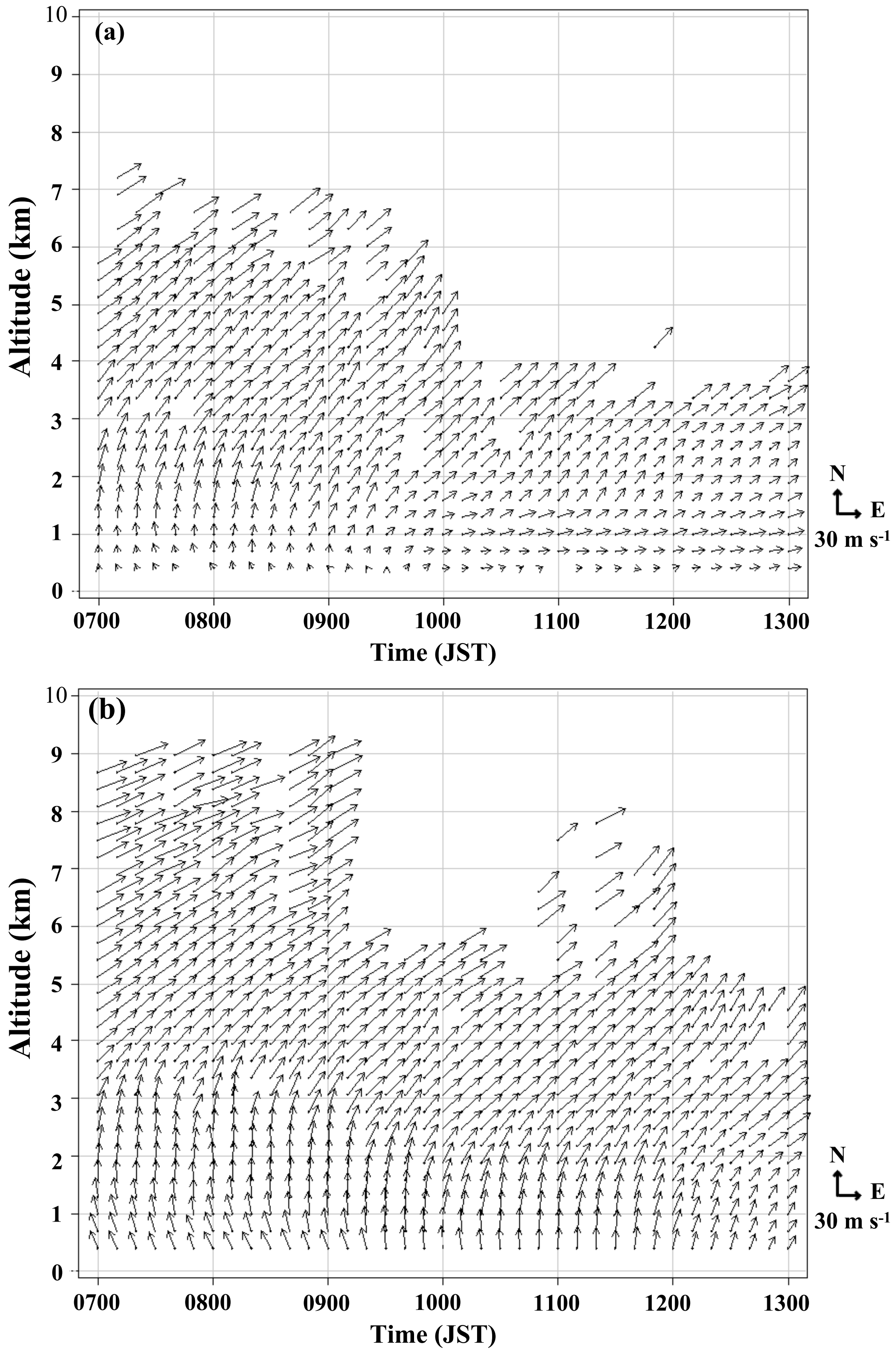

Figure 4.6. The time-height cross section of horizontal wind observed from 0900 to 1500 JST on 8 Apr, from WINDAS site at (a) Takamatsu, (b) Mihama.

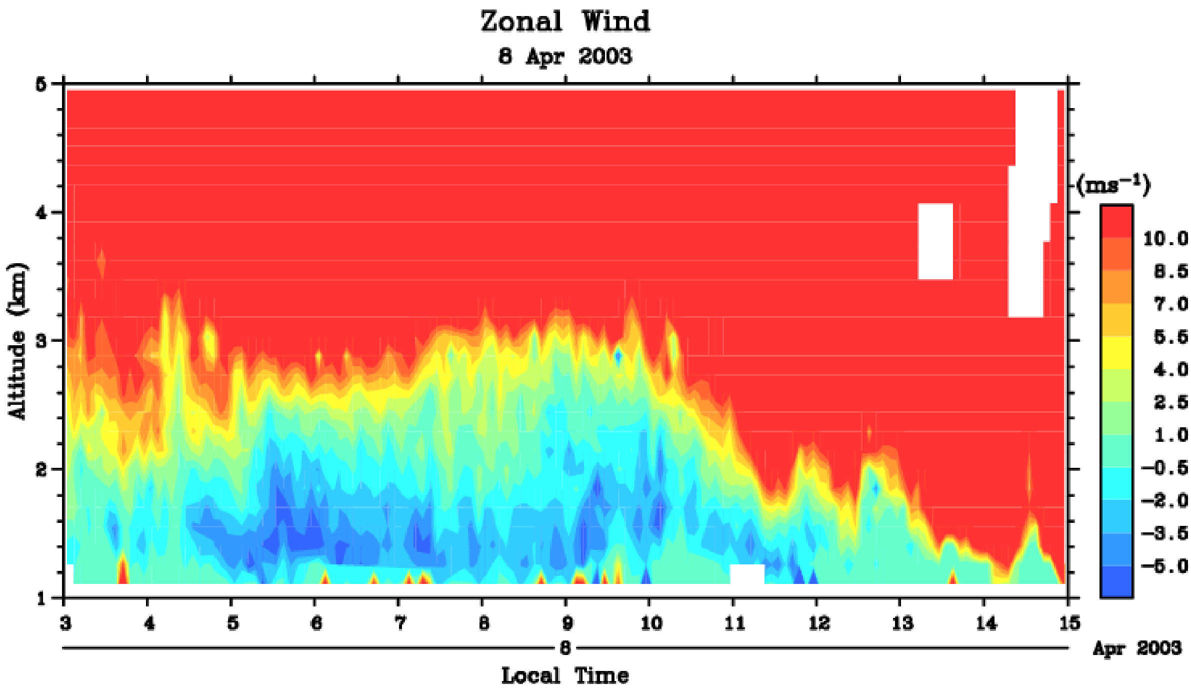

Figure 4.7. Zonal wind observed by MU radar from 0300 to 1500 JST on 8 Apr. Contour is the wind speed (Minus value indicated easterly component and plus value is westerly component).

4.1.3 Discussion

Okumura and Satomura (2001, private communication), and Arai et al. (2001, private communication) used the operational observation network including an X-band Doppler radar and showed that band-like structures appeared near the cold front extended south-ward or southwest-ward from the Sea of Japan to the Honshu Island and westerly wind was dominant in a meso-α-scale area at 3 km altitude. However, in 1998 case, we did not appear to the westerly wind. The southerly wind (about 10 m s^{-1}) was dominant around Kii Channel in the period. The line-shaped precipitation band was stationary from 1800 to 2400 JST. The band position was coincided the Rokko mountain. Kato (2005) pointed that the orographic effect and the southwesterly wind which speed is between 5 and 25 m s^{-1} at 850-hPa-level is important in stagnant precipitation band in Kyusyu. We consider that the southerly wind was arrived to Rokko Mountain, since the southerly wind was not blocked by the westerly wind. If the air parcel was ride over the Rokko Mountain, the air parcel was condensed easily because the LCL is 957-hPa level and the LFC is 922-hPa level. On the other hand, we appear to the southeasterly wind existed from Ise Bay in 2003. In this case, the line-shaped precipitation band was stagnant from 1000 to 1300 JST. Konishi and Umemoto (2001, private communication) pointed that the warm moist air mass were intruded over Kii Channel or Ise Bay before precipitation started. We observed the southeasterly wind around MU radar site and we clarified a meso-β-scale low in Kii Peninsula. We consider that the meso-β-scale low is role of making southeasterly wind. The meso-β-scale low in Kii Peninsula is located the lee side of Kii mountains. The southeasterly wind was dominant from 0500 to 1200 JST below 2 km altitude. The line-shaped precipitation band was stagnant until the southeasterly wind was disappeared. Therefore the two line-shaped precipitation bands was influenced directly or indirectly orographic effect.

4.2 Case studies in 2006

4.2.1 Major features of line-shaped precipitation bands in Kinki District

Figures 4.8 (a) and (b) show distributions of precipitation intensity from 0920 to 1100 JST on 2 July 2006 and from 2120 and 2300 JST on 5 July 2006. On 2 July, a line-shaped precipitation band with precipitation intensity exceeding 30 mm h^{-1} was formed in the northeastern side of Osaka Bay at 0940 JST, and was maintained until 1100 JST. On 5 July, an area of rainfall exceeding 30 mm h^{-1} was formed at 2140 JST around Osaka Bay, and was maintained with moving eastward until 2240 JST.

Figure 4.9 shows weather maps at 0900 JST on 2 July and 2100 JST on 5 July. There were features common in both the two cases. At surface, a meso-α-scale occluding cyclone with a central pressure of 996 hPa existed over the Sea of Japan. A cold front extending from the occluded point was located over Kinki District. A trough axis was located along 135°E at 850-hPa level, and it was shifted westward at 500-hPa level. A horizontal wind shear was seen around this trough, and southwesterly was strong in the eastern side of the trough at 850-hPa and 500-hPa levels. At this time, Kinki District was located in the eastern side of the trough, where the west-southwesterly speed was 20–30 m s^{-1}. As shown in Fig. 4.10, the trough was clear at 700-hPa level, and the line-shaped precipitation band appears when the trough approached Kinki District.

In the MANAL data is shown in Figs. 4.11. We find again common features in the mesoscale for the two cases of 2 and 5 July. A meso-β-scale low existed in the eastern part of Shikoku Island. Strong southwesterly appeared to east of the low, where equivalent potential temperature (θ_e) was higher (>345 K) at the 950-hPa level. The high θ_e area covered the areas where the line-shaped precipitation bands shown in Fig. 4.8. The northwest edge of the high θ_e area was close to the northwestern side of a precipitation band. These results suggest that southwesterly wind intensified by the meso-β-scale low plays an important role to transport warm and moist airmass from the south to the line-shaped precipitation band.

The lowest atmosphere around Osaka Bay is investigated using the vertical cross-sections of θ_e. Figure 4.12 shows the vertical latitude-height cross sections of θ_e and horizontal wind along 135.2°E (line S−N in Fig. 4.10) based on the MANAL. In both the two cases, the high θ_e air (> 345 K) and southwesterly wind (about 20 m s^{-1}) existed below approximately 950-hPa level. Therefore the lowest atmosphere from 34.0°N to 34.8°N was strongly convectively unstable. At 2100 JST 5 July shown in Fig. 4.12 (b), a neutral stratification region existed vertically up to 500-hPa level from 34.0°N to 34.5°N, because the convection had already been started at the time of the MANAL data analysis.

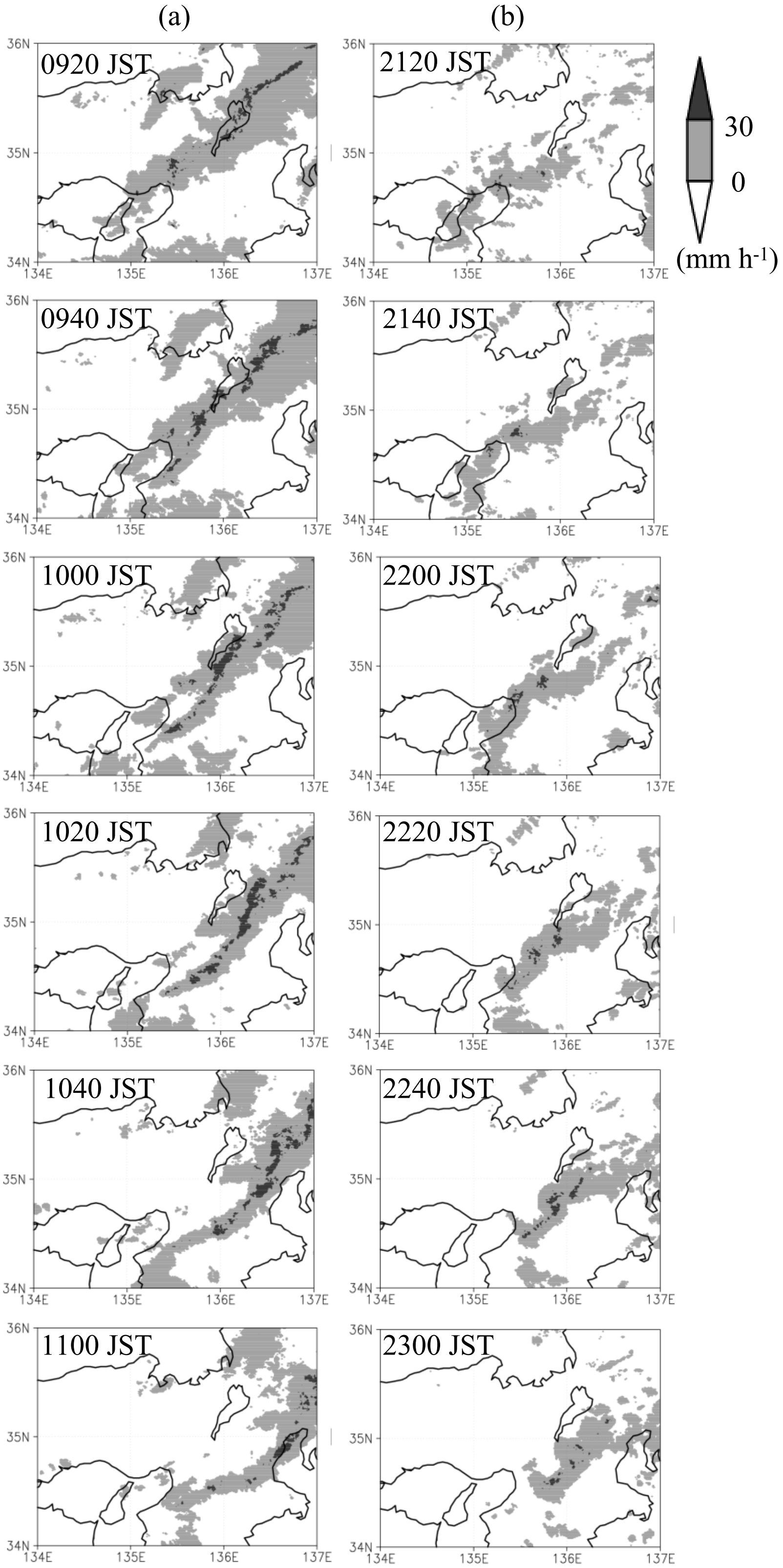

Figure 4.8. Horizontal distributions of precipitation echo intensity at 2 km height level observed by the JMA operational radars (a) from 0920 to 1100 JST on 2 July 2006 and (b) from 2120 to 2300 JST on 5 July 2006. Time interval is 20 minutes.

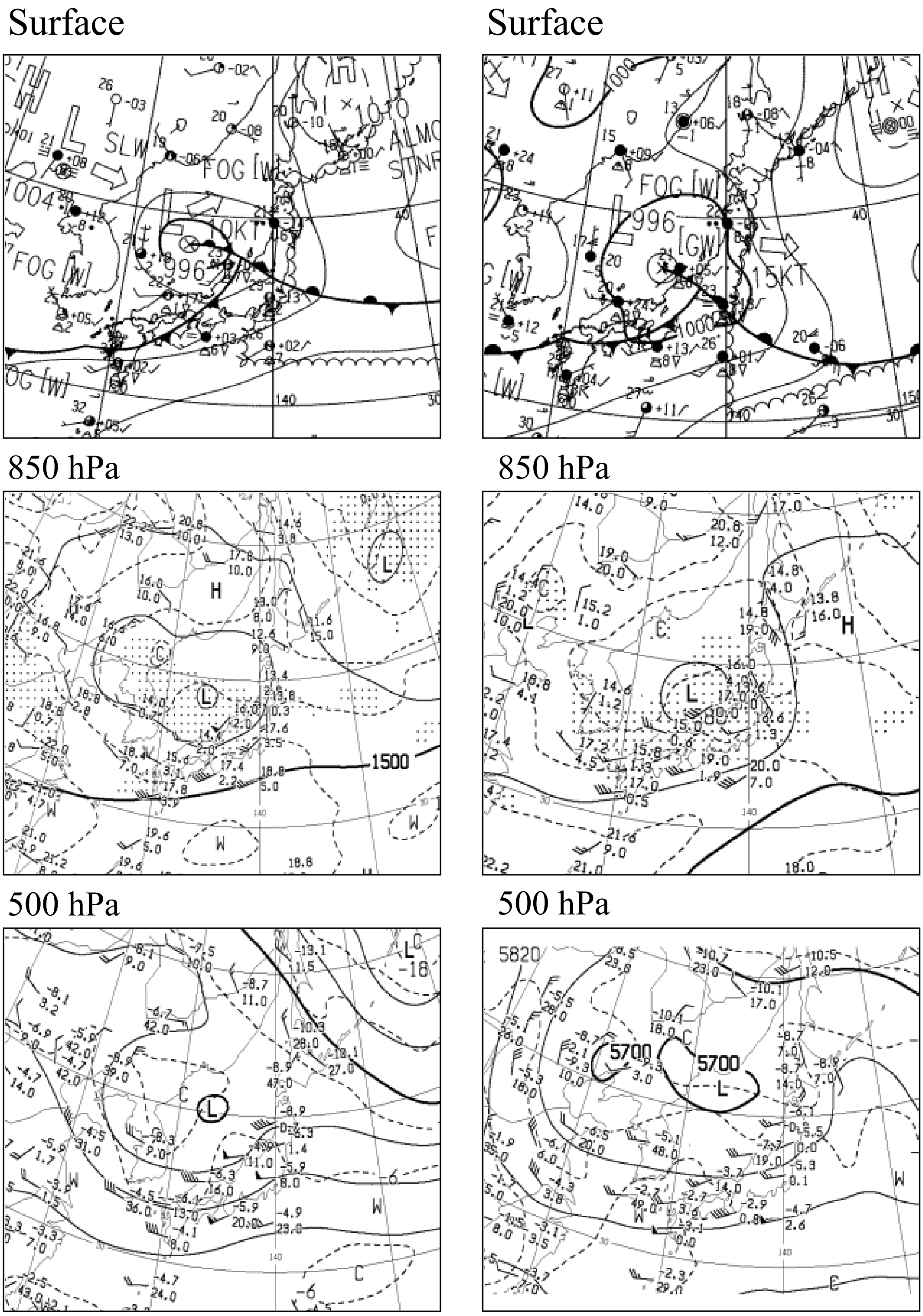

Figure 4.9. Weather maps of surface, 850- and 500-hPa levels at 0900 JST on 2 July (left-hand side panels) and 2100 JST on 5 July (right-hand side panels). In the 850- and 500-hPa levels weather maps, solid and dashed lines indicate geopotential height (m) and temperature (°C). In 850-hPa level, the dotted area is wet area ($T - T_d \leq 3$ °C).

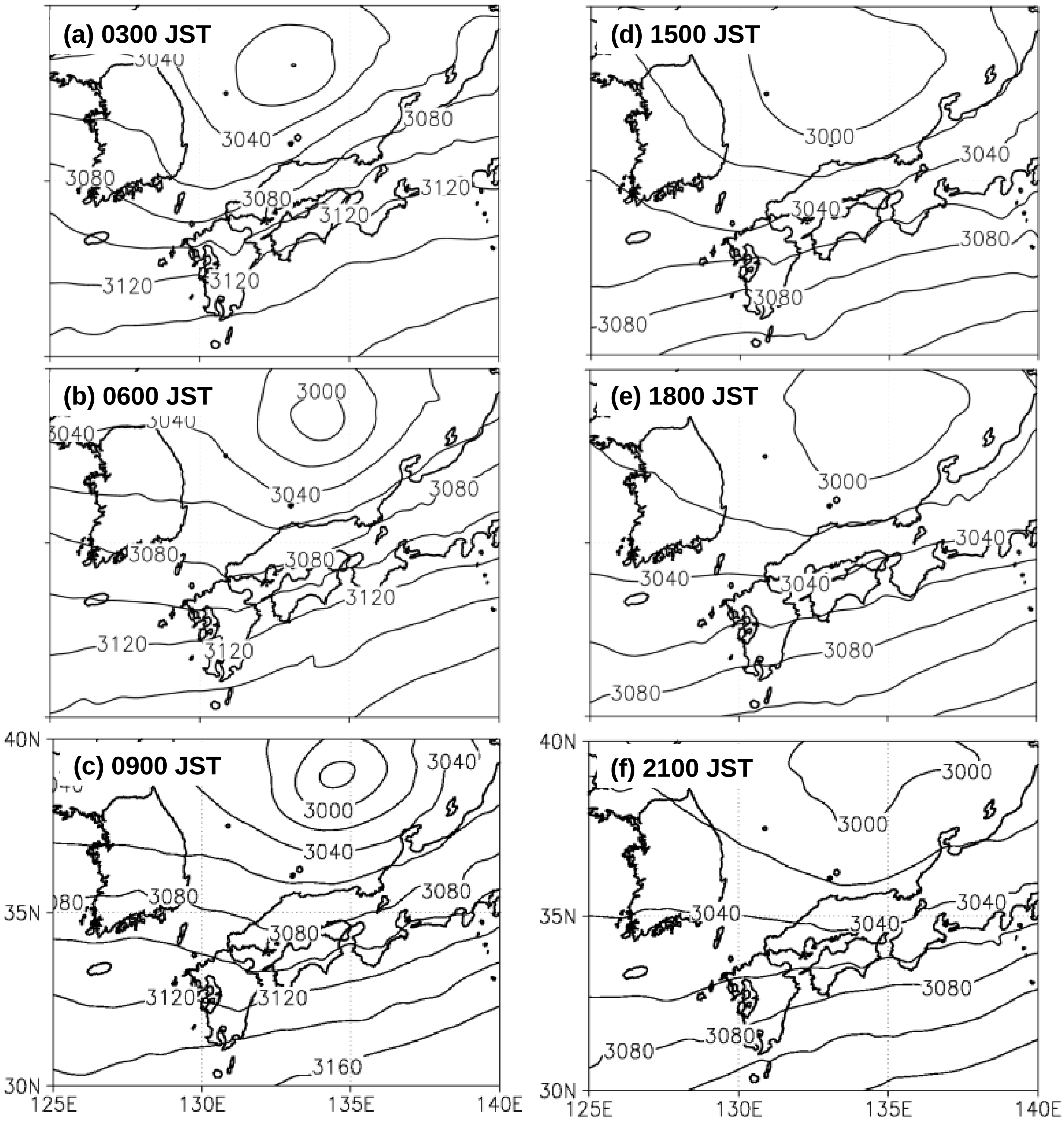

Figure 4.10. Geopotential height (m) at 700-hPa level. (a)-(c) are 2 July, (d)-(f) are 5 July.

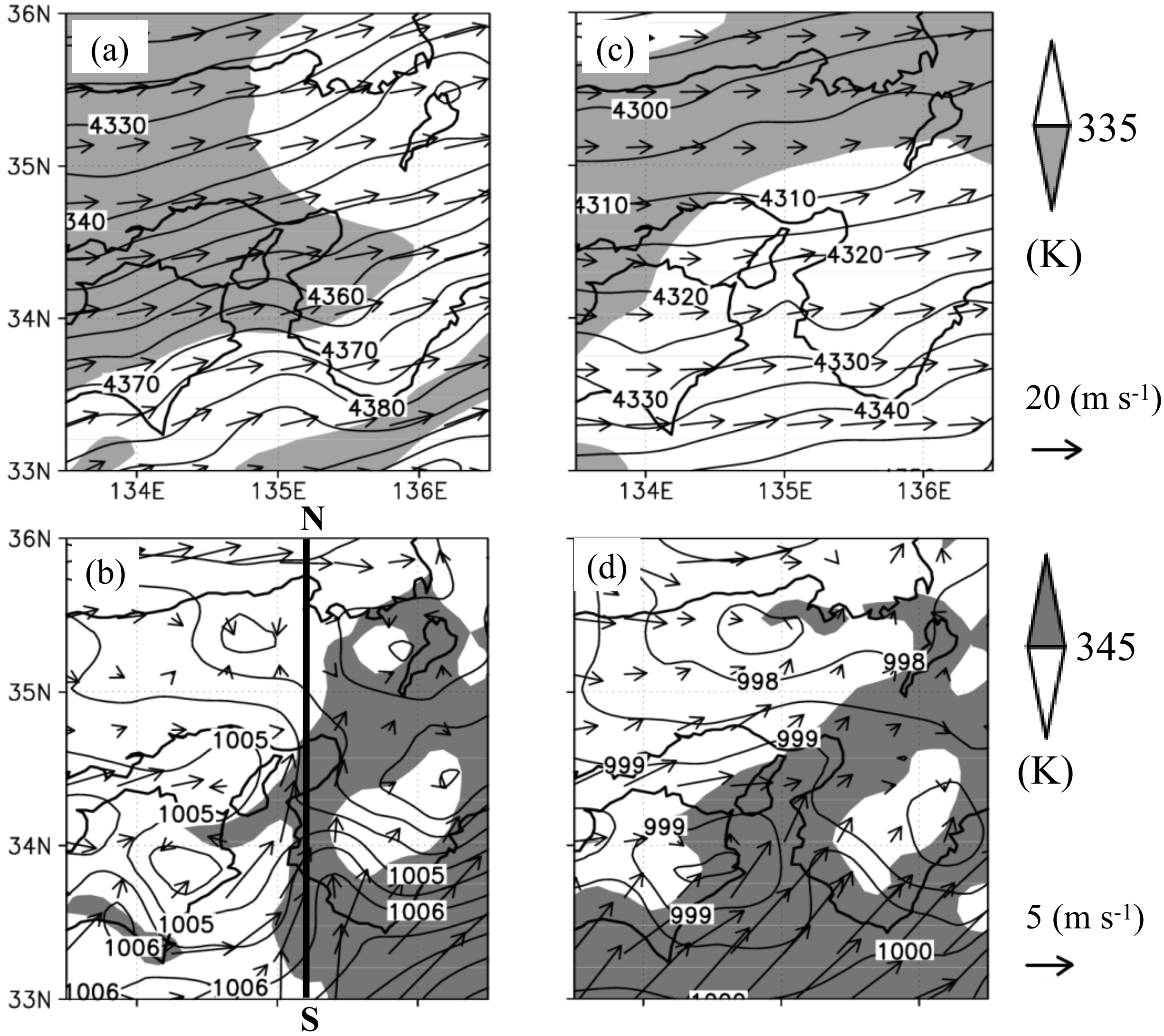

Figure 4.11: (a) 600- and (b) 950-hPa levels equivalent potential temperature (θ_e) fields at 0900 JST on 2 July. Contours show (a) geopotential height (m) and (b) sea level pressure (hPa). Arrows indicate (a) 600-hPa and (b) surface wind (m s^{-1}). (c) and (d) are same as (a) and (b) but for 2100 JST on 5 July.

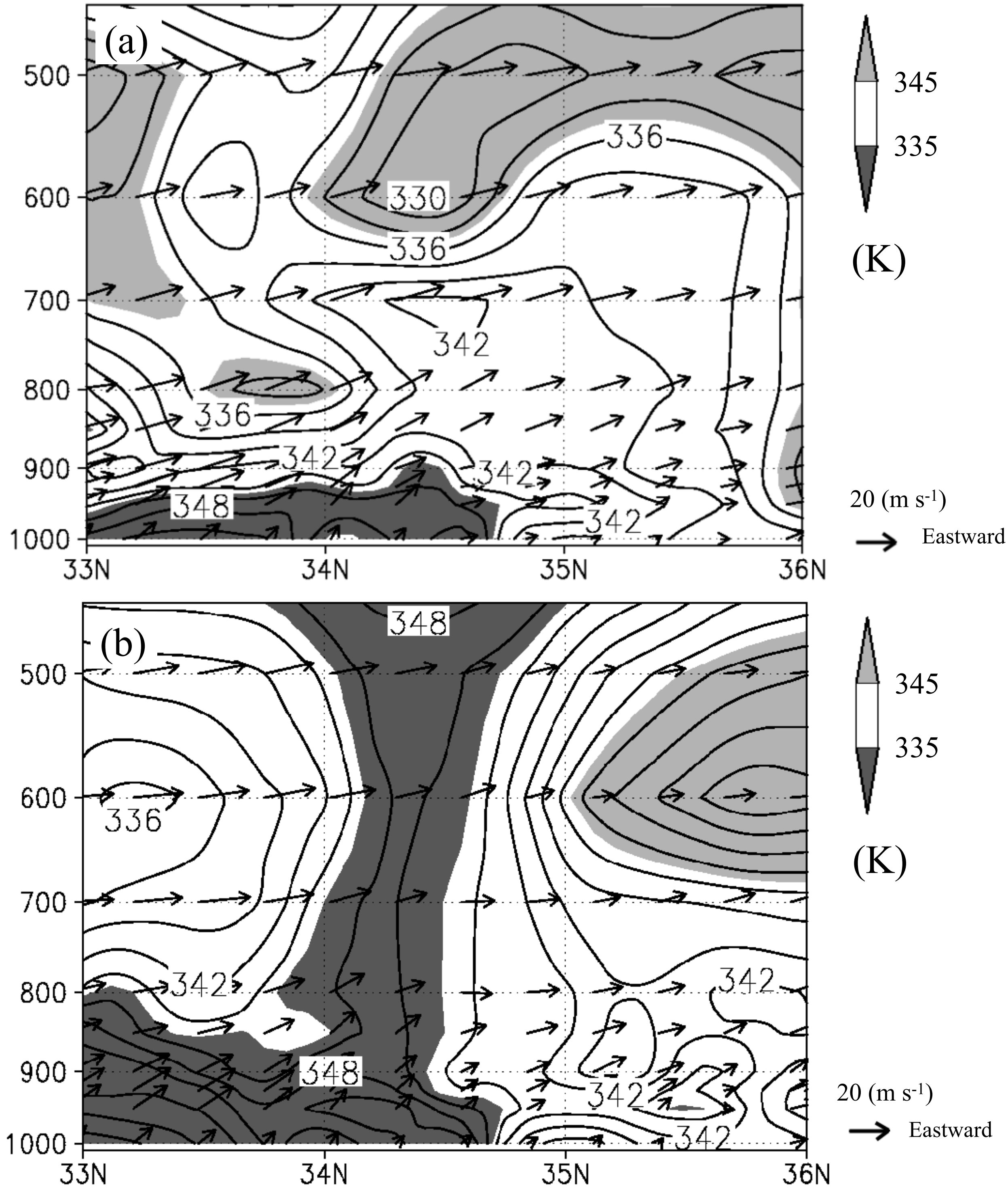

Figure 4.12. Meridional-vertical cross sections of equivalent potential temperature (θ_e) and horizontal wind (upward is northward) along 135.2°E (corresponding to the line S–N in Fig. 5) at (a) 0900 JST on 2 July and (b) 2100 JST on 5 July. The data have been taken from the MANAL.

4.2.2 Meso-β-scale low ("Tokushima small low")

In Fig. 4.11b and d, a meso-β-scale low is found near Tokushima in the eastern part of Shikoku Island for the two cases of 2 and 5 July. Hereafter this meso-β-scale low is named as "Tokushima small low". Strong southwesterly appeared to the east of the low, where θ_e was high (>345 K) at the 950-hPa level. This result suggests that the southwesterly intensified by the Tokushima small low played an important role to transport warm and moist air mass from the south to the line-shaped precipitation band.

Figure 4.13 shows temporal and spatial distributions of 3-hourly pressure and horizontal wind at surface level on 2 and 5 July. From this figure, it is confirmed that the life time of the Tokushima small low was about 6 hours. Meso-β-scale wave-like disturbances with a horizontal wavelength of about 200 km are also found in the pressure field from Shikoku Island to Kii Peninsula. The meso-β-scale waves appeared before the Tokushima small low. The amplitude was increased when the Tokushima small low was developed. As a result, the southwesterly wind intensified over the Kii Channel while the Tokushima small low developed.

In July ddring the five years surveyed in the previous subsection, the Tokushima small low was formed four times (12 July 2005, 2 July 2006, 5 July 2006, and 21 July 2006). In all the four cases the Tokushima small low was stagnant for several hours, and had a central pressure lower by about 1 hPa than the surrounding pressure field. These four cases were included in the 15 cases of passages of cold fronts extended from meso-α–scale cyclones. Even when the meso-α-scale cold front passes around Osaka Bay and also the Tokushima small low was formed, the line-shaped precipitation was not always formed.

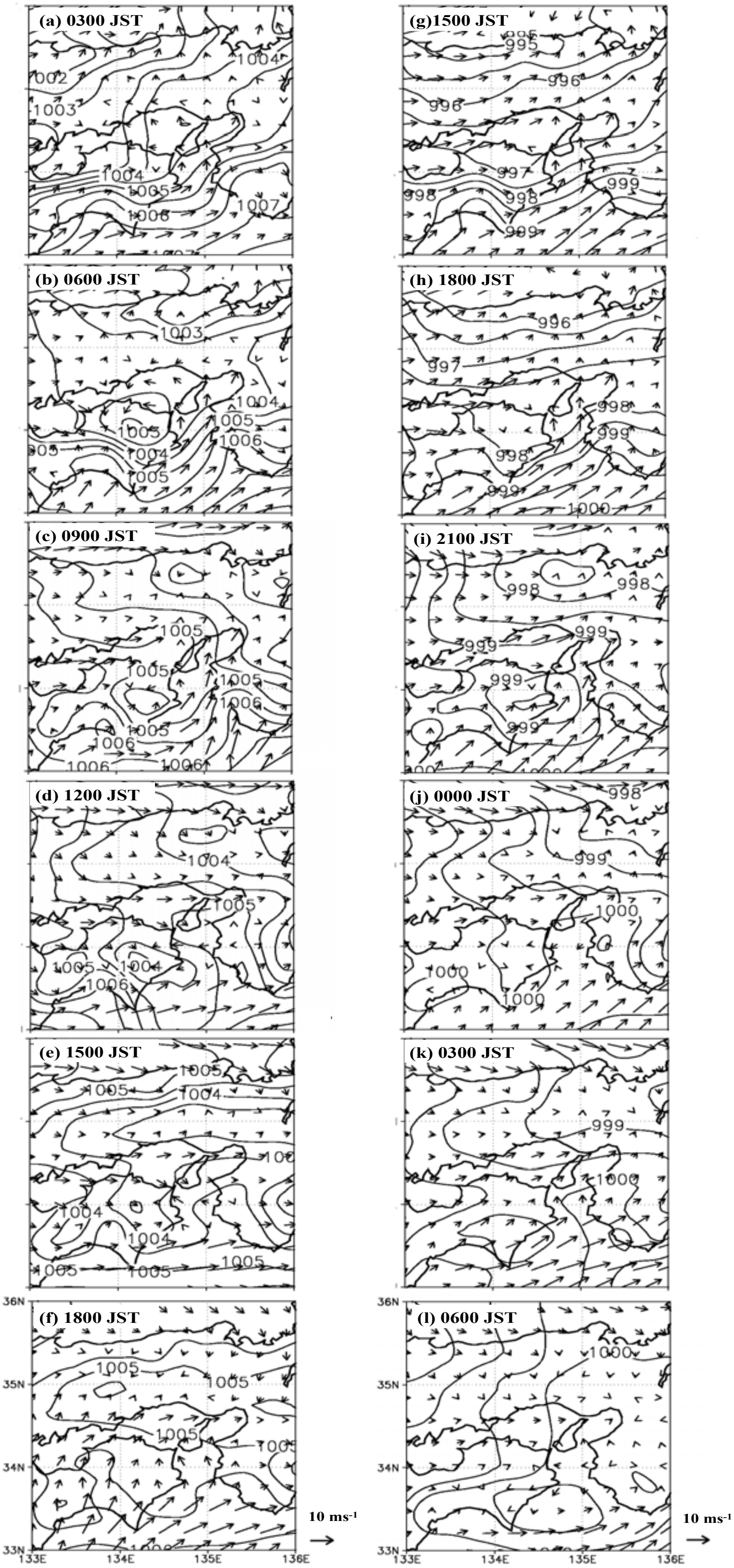

Figure 4.13. Sea level pressure (hPa) and surface wind (m s^{-1}). The left-hand side panels are 2 July from0300 to 0900 JST, the right-hand side panels are 5 July from 1500 to 2100 JST.

4.2.3 Wind distribution near the line-shaped precipitation bands

As mentioned in previous subsections (see Figs. 4.9–4.13), on one hand, southwesterly of 10–15 m s^{-1} intruded from south into Osaka Bay below 900-hPa level at 0900 JST on 2 July and at 2100 JST on 5 July. On the other hand, westerly was dominant over Seto Inland Sea located to the west of Osaka Bay. As a result, convergence of these westerly and southwesterly appeared in the western (colder) side of the cold front passing Osaka Bay, which might be suitable to develop convection such as the line-shaped precipitation band shown in Fig. 4.8.

The westerly was gradually increased with height up to a jet stream (about 25 m s^{-1}) between 700- and 600-hPa levels. Southerly was relatively strong (10 m s^{-1}) below 800-hPa level between 135°E and 136°E, and northerly (2–4 m s^{-1}) appeared below 900-hPa level between 134°E and 135°E (not shown). These wind behaviors show that the horizontal wind field had a strong vertical shear with clockwise rotation near the line-shaped precipitation bands.

At Takamatsu located to the west of the precipitation band (see Fig. 4.14), the wind profiler data show that southwesterly below 1.5 km (about 850 hPa) was changed to westerly around 0800 JST on 2 July and around 2000 JST on 5 July, suggesting cold front passages. In the vertical structure, wind direction rotated clockwise with height from the southwesterly below 900-hPa level to westerly at higher levels, in particular near the line-shaped precipitation band (34°–35°N), as shown in Fig. 4.9. Comparing hodographs of horizontal wind observed by the wind profiler at Takamatsu and by a rawinsonde at Kobe (see Fig. 4.15) a clear clockwise rotation is found at Kobe in the eastern (leeward) sides of westerly flowing beyond mountains of Awaji Island than at Takamatsu in the western (windward) side. The clockwise rotation of wind direction with height is also known as a feature of upward propagating internal gravity waves (see, e.g., Yamanaka et al. 1995; Ogino et al. 1999), although at this stage we cannot decide whether such gravity waves are a cause or a result of the line-shaped precipitation band.

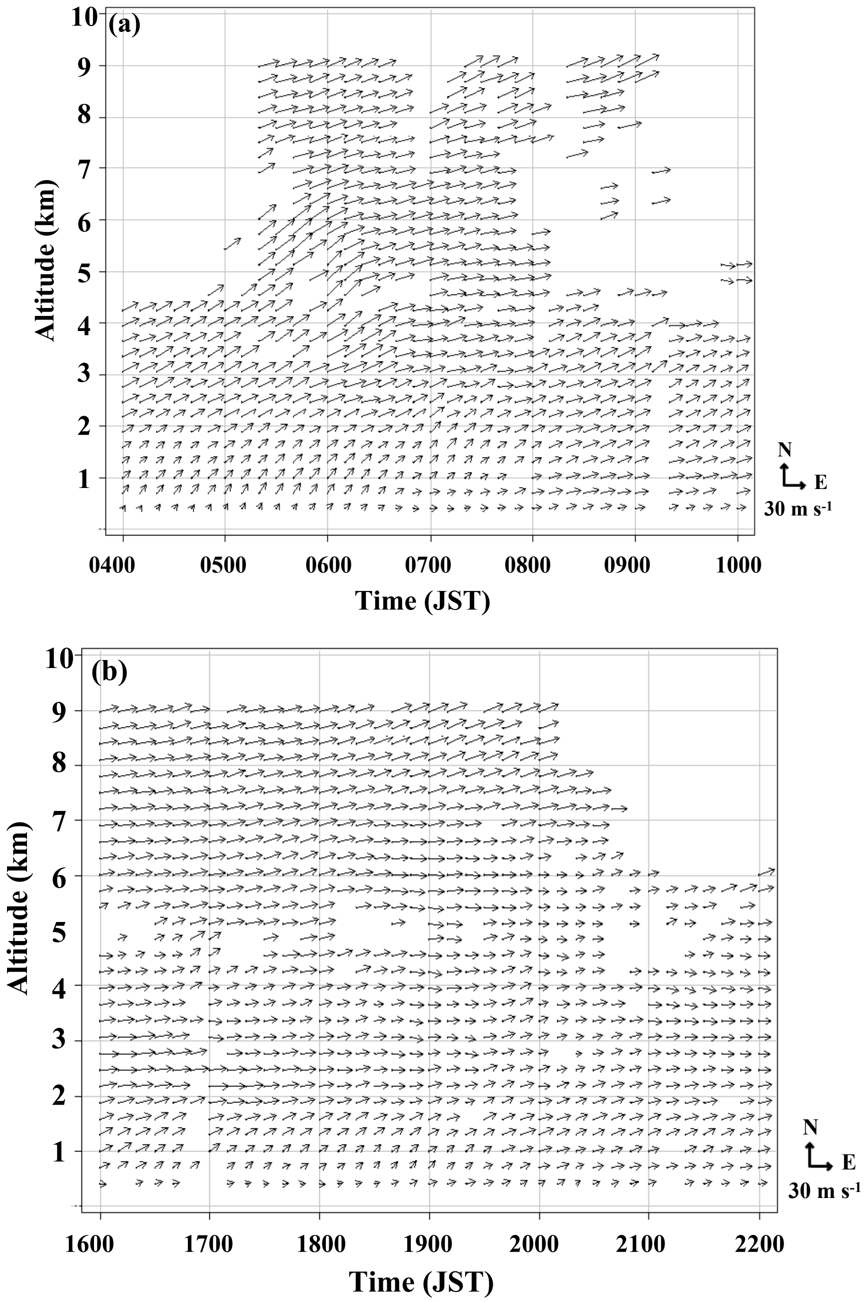

Figure 4.14. The time-height cross section of horizontal wind observed at Takamatsu WINDAS site (a) 2 July and (b) 5 July.

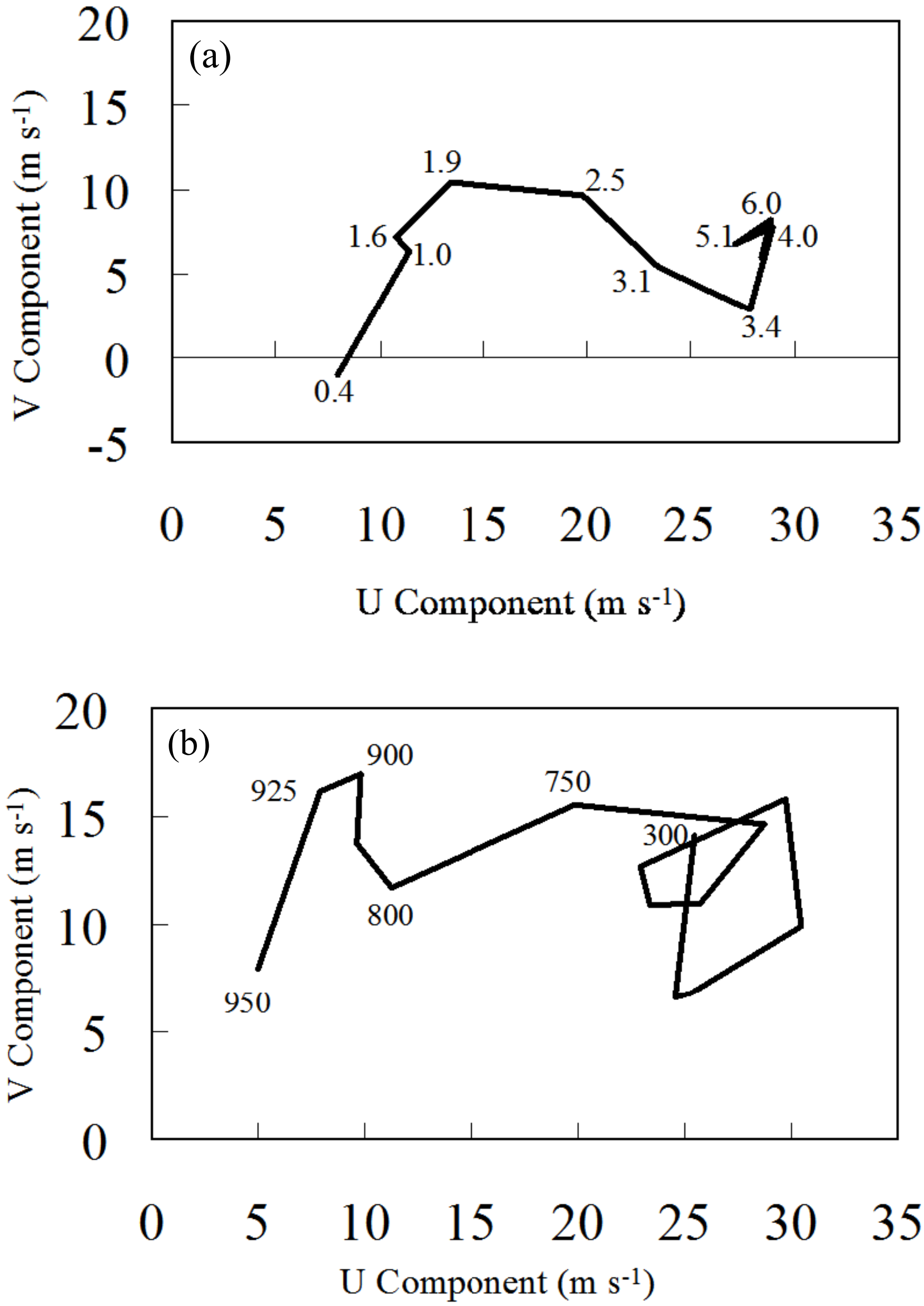

Figure 4.15. Hodograph of horizontal wind at (a) Takamatsu in 0650 JST by Wind profiler, and (b) Kobe University in 0652 JST by rawinsonde on 2 July. The number in figures indicates (a) altitude (km), and (a) pressure levels (hPa). U and V are the east-west and the south-north components, respectively.

Chapter 5

Numerical study and discussions

5.1 Numerical simulation

Temporal changes of horizontal distributions of horizontal wind and hourly-accumulated precipitation simulated by MM5 are shown in Fig. 5.1. For the case of 2 July, the simulation successfully reproduces the temporal/vertical changes of horizontal wind observed at Takamatsu wind profiler (Fig. 4.14 (a)) and the line-shaped precipitation band observed as the radar echo areas (Fig. 4.8(a)). For the case of 5 July, the simulation was successful, although the simulated rainfall area is slightly south from observed one shown in Fig. 4.8(b). Therefore, we can investigate the line-shaped precipitation band around Osaka Bay by these simulation data with temporal and horizontal resolutions higher than by MANAL data, in particular concerning detailed wind field. As mentioned in previous subsections, the westerly and southwesterly dominant to the west and east, respectively of the cold front may make a convergence of meso-α- or -β-scale, but the sharp convergence zone representing in results of the numerical model (Fig. 5.1) is clearly smaller, that is, of meso-γ-scale. Therefore, we need to consider other mechanism which is different from the meso-α- or -β-scale wind field, in order to explain generation of such a meso-γ-scale convergence zone which should be corresponding to the line-shaped precipitation band.

In the zonal-vertical cross sections of potential temperature (θ), cloud water and zonal-vertical wind along 34.5°N for the two cases of 2 and 5 July, (Fig. 5.2) we find meso-γ-scale mountain waves in the leeside of Awaji Island and larger cloud water amount in updraft areas of the windward side and of the mountain waves in the leeside. Similar features are seen near another island (Shodo Island) to the west of Awaji Islands but the cloud water does not increase so much. This difference is due to the moisture distribution which is shown clearly in the zonal-vertical cross sections of θ_e and mixing ratio (Fig. 5.3). The larger moisture is eastern side of partly due to eastward moving cold front which appears as strong gradients of θ_e and mixing ratio, and the particularly large moisture in the leeside of Awaji Island is due to water vapor transport by southwesterly intensified by the Tokushima small low.

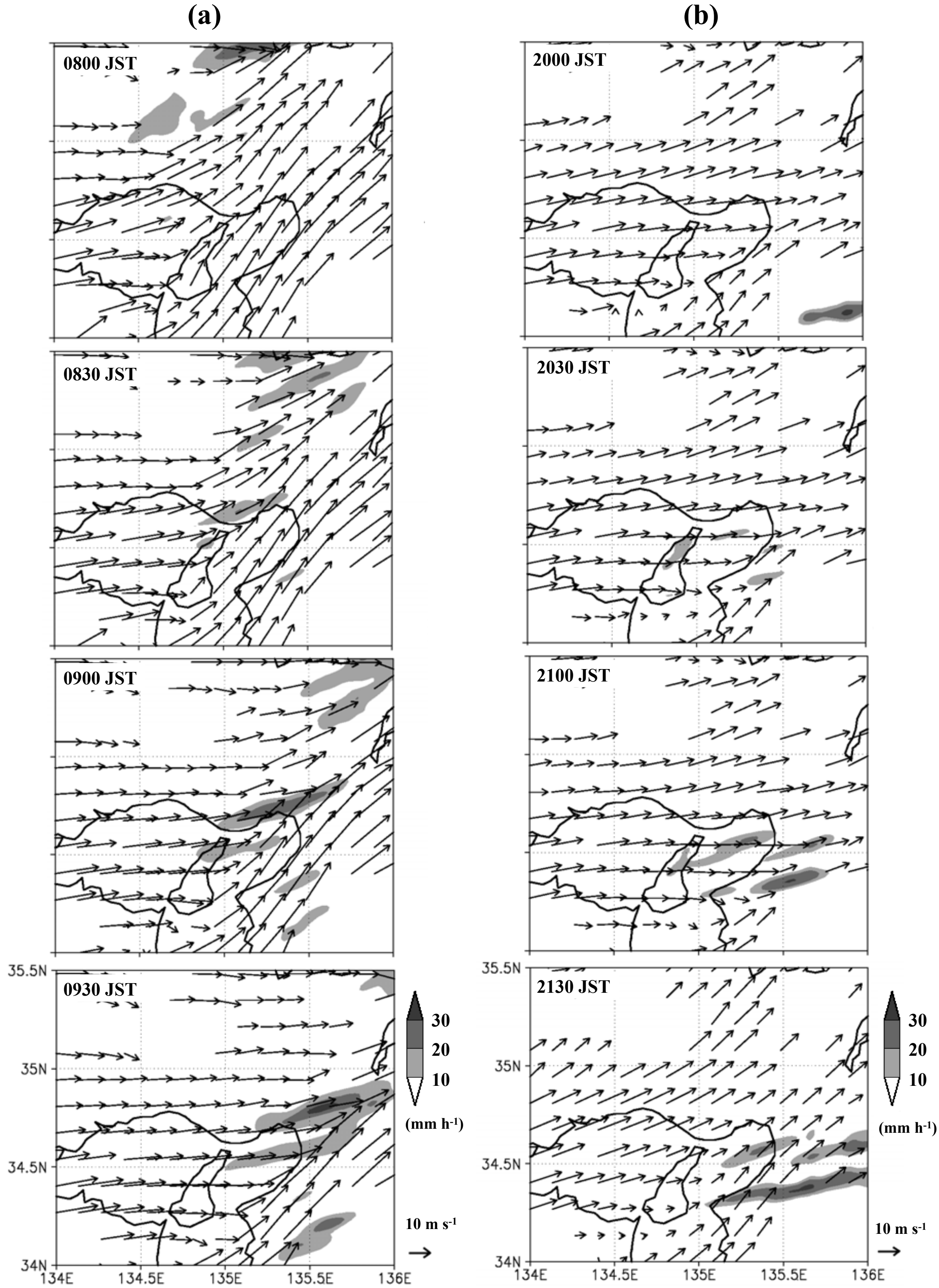

Figure 5.1. Horizontal distributions of 950-hPa level wind and hourly precipitation (between 30-min before and after each time) simulated by MM5 for the cases of (a) 2 July and (b) 5 July.

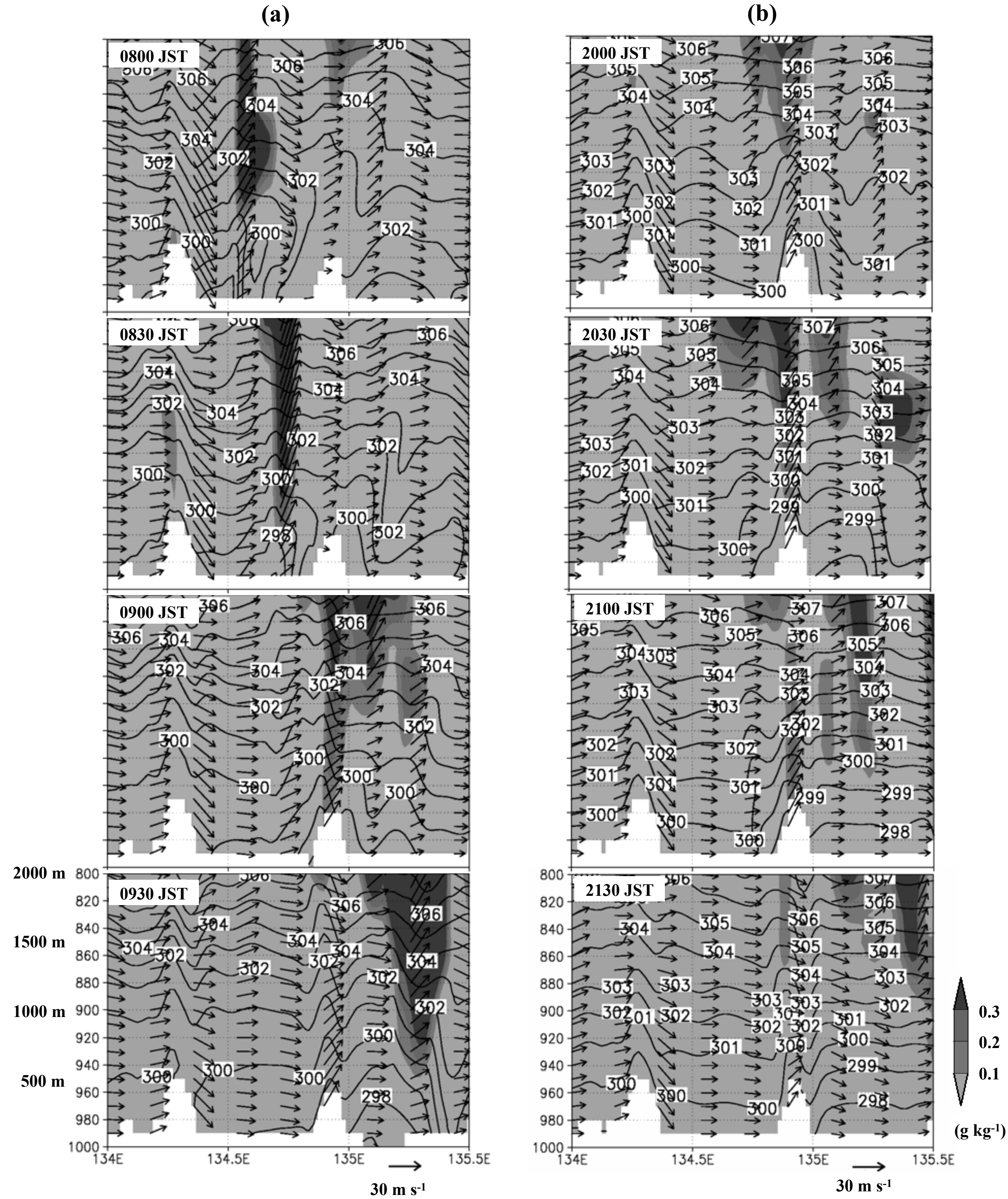

Figure 5.2. The horizontal-vertical cross sections of equivalent potential temperature, cloud water and zonal and vertical winds along 34.5°N for the cases of (a) 2 July and (b) 5 July, based on simulated by MM5

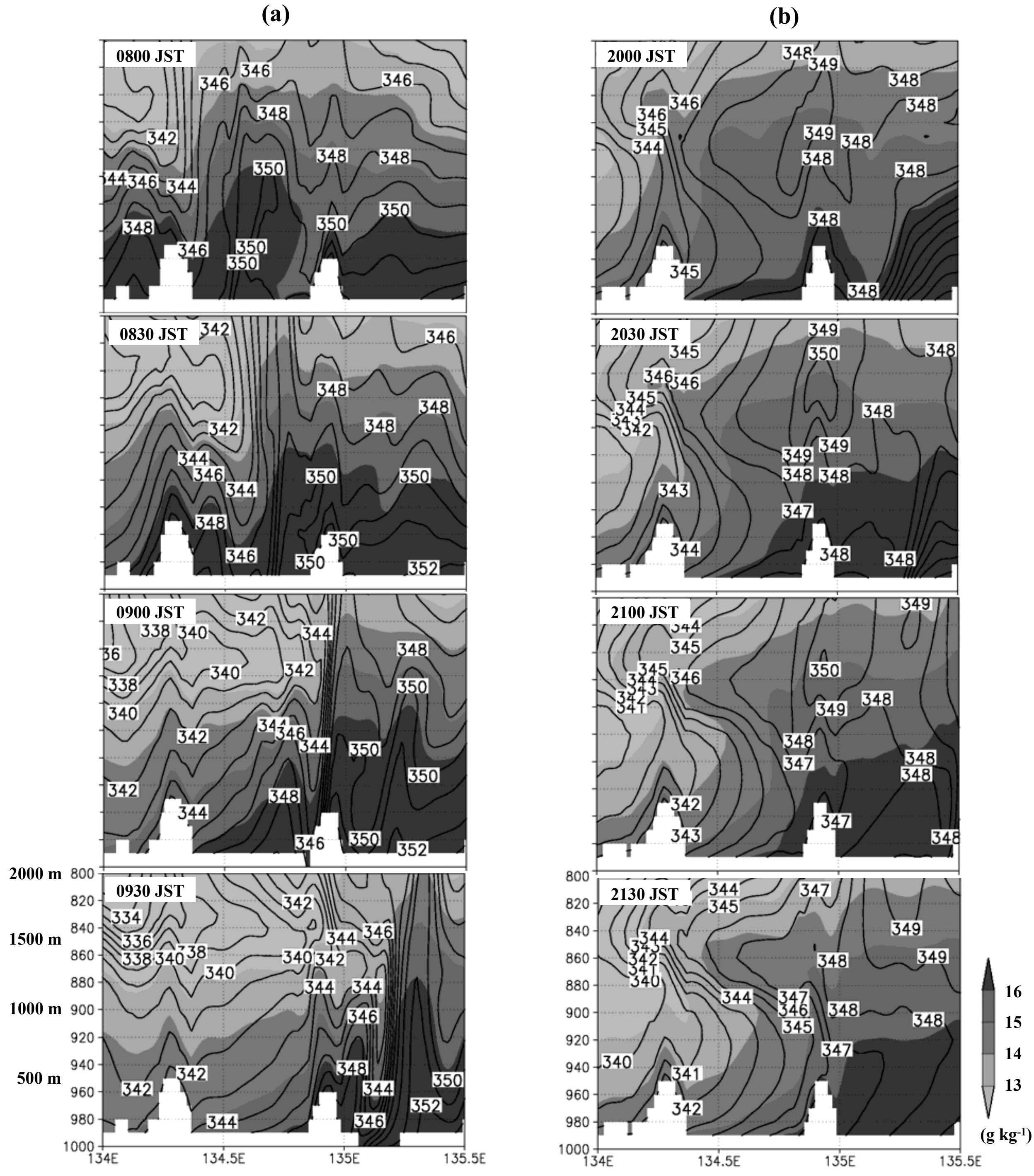

Figure 5.3. The horizontal-vertical cross sections of equivalent potential temperature and mixing ratio along 34.5°N for the cases of (a) 2 July and (b) 5 July, based on simulated by MM5.

5.2 Cold front and jet stream in the late Baiu season

It has been known that meso-α-scale cyclones develop on the Baiu frontal zone (Yoshizumi 1977). Some troughs associated with the meso-α-scale cyclones incline eastward with increasing height, corresponding to a thermo dynamical structure that cold air exists on the east side of a trough in the lower atmosphere (below 800-hPa level), and the low-level wind and horizontal temperature gradient are weaker than the other cases of troughs (as usual synoptic-scale cyclones) inclining westward with increasing height. The troughs of the two cases generating line-shaped precipitation bands in late Baiu season inclined westward with increasing height (see Fig. 4.9), and have a cold front with relatively strong vertical wind shear and horizontal temperature gradient in the lower layer.

The low-level jet stream (Ushijima 1969, Mohri 1956), or Baiu jet (Kato et al. 2003) appears around Baiu front in particular near heavy rainfall areas (Ninomiya and Akiyama 1974), and makes strong vertical wind shear necessary to develop cumulus convection (Beebe and Bates 1955). In the present cases, a zonal wind maximum appeared between 700- and 600-hPa levels at 34.5°N, and another upper-tropospheric jet stream with wind speed of 20–30 m s^{-1} existed over west Japan (cf. Fig. 4.14). We considered that this strong wind contributed mainly the meso-α-scale cyclone-front system development.

In the present cases, convergence between southwesterly of 10–15 m s^{-1} induced by meso-β-scale low below 900-hPa level, and westerly induced by meso-α-scale front-cyclone system looks directly important to make strong instability as mentioned in sections 4.2.3-5.1. As Ninomiya (1978) persisted, the destabilization of the stratification on the heavy rainfall area is not caused by the cold air intrusion aloft but mainly by the intrusion of the tropical air mass in the lower layer. Kato and Aranami (2005) showed that Niigata-Fukushima and Fukui heavy rainfalls in Honshu Island resulted from intensification of convective instability over the Baiu frontal zone, induced by the inflow of the low-level (925-hPa level) humid air and the middle-level (500-hPa level) dry air. The middle-level (500-hPa level) air was considerably warm and not colder than the surrounding air, which indicates that the formation factors of heavy rainfalls should be examined using convective instability, rather than potential instability. Kato and Goda (2001) and Kato (2006) showed that in case of heavy rainfalls in Niigata and Fukuoka the convective instability was maintained in the low-level (950- or 925-hPa level) humid air ($\theta_e > 340$ K) and the dry air ($\theta_e < 330$ K) come from 600-hPa level to 500-hPa level. In our case, the middle-level (600-hPa level) low θ_e (< 335 K) air was caused by the dry air (< 5 g kg^{-1}) which was not colder than the surrounding atmosphere.

Based on the observational evidence described in the previous section, a line-shaped precipitation band is developed around Osaka Bay by the following three processes; in meso-α-scale, as suggested by some previous studies convective instability is induced by a cold front; in meso-β-scale, the instability is intensified by low-level moist air ($\theta_e > 345$ K below 950-hPa level) with southwesterly wind in the east of an orographic low in Shikoku Island; and in meso-γ-scale, the rainfall becomes intensifying by lee waves of mountains in Awaji Island and/or Rokko Mountains.

In this section, we discuss these three conditions by using numerical models. Existence of the lower-level southerly (< 900-hPa level) below the Baiu jet westerly (around 700-hPa level) over the Osaka Bay produces a strong wind shear (rotating clockwise with height) is a suitable condition for generation of the line-shaped precipitation band (e.g., Alexander and Young 1992; LeMone et al. 1998).

5.3 Formation of Tokushima small low

Yamakawa (1980) and Sakakibara (1983) showed that a small (meso-β-scale) low enhanced by surface (solar) heating to west of Kanto area below 500-hPa level intensified warm moist southerly/southeasterly, which was weak (< 15m s^{-1}) in the meso-α-scale filed, and enhanced precipitation systems near a cold front by producing a large temperature gradient in the zone to the northeast of the low. In the present cases, we have found out the Tokushima small low with a diameter of about 200 km, which appeared during the cold front passage and remained stationary for about 6 hours. However, concerning the origin of the Tokushima small low, the surface heating with the solar radiation does not seem to be so important, because the low was formed in early morning or after sunset.

Before the Tokushima small low appeared, stationary wavy structures of meso-β-scale were also generated in a zone of dense isobar distribution along the southern coasts of Shikoku Island and Kii Peninsula (see Figs. 4.11 and 4.12). After that, the Tokushima small low appeared, and in front of a trough produced by these wavy structures, the pressure gradient became as strong as about 1 hPa/50 km, which corresponded to a geostrophic wind of about 19 m s^{-1}, although the actual wind was not exactly in a geostrophic balance. To discuss the orographic effect of Shikoku Mountains on the strong lower-level wind, we calculated the local Froude number defined by

$$Fr = \frac{U}{N \cdot h}, \tag{1}$$

where

$$N = \left[\frac{g}{\theta} \cdot \frac{\partial \theta}{\partial z} \right]^{\frac{1}{2}} \tag{2}$$

is Väisälä-Brunt frequency, g is gravitational acceleration, h is mountain height and U is environmental wind speed (e.g., Wang and Chen 2003). Specifying U and N by the MANAL wind data averaged for 16 grid points near the southern coast of Shikoku Island (see Fig. 2.6), we obtain $Fr \sim 1$ for air parcels in the windward side of Shikoku Mountains for the four cases in which the Tokushima small low was generated (see Table 5.1). This implies that air flow may rise over (above 900-hPa level) and/or go around (below 900-hPa level) the mountains (Smolarkiewicz and Rotunno 1989, 1990).

5.4 Effect of lee waves

We have noticed in Subsections 4.2 the possibility of contribution of lee waves generated by Awaji Island. In this case, we have $Fr \sim 4$ (>1), for $U \sim 15$ m s^{-1}, $N \sim 10^{-2}$s^{-1} and $h \sim 400$m, and the windward air may climb the mountains of Awaji Island and generate lee waves.

From Fig. 5.2, the typical wavelength of the lee waves was 15–20 km and the amplitude was 500 m. If we assumed the liner theory, the critical (largest) horizontal wavenumber is given by a square root of the Scorer parameter (l^2):

$$l^2 = \frac{N^2}{U^2}. \tag{3}$$

We specify $U \sim 15$ m s^{-1} by the averaged wind at 950-hPa and $N \sim 10^{-2}$ s^{-1} by Fig. 11, and estimate the shortest wavelength $2\pi/l \sim 9$ km. Therefore observed lee waves with 15–20 km wavelength may be propagating vertically as internal gravity waves.

The conditionally unstable layer existed over Osaka Bay, and the lifting condensation level (LCL) computed from our rawinsonde observation data was located at around 950-hPa level. Because the wave amplitude of isentropic surface was 500 m, the air parcel reached easily the LCL. Therefore we consider that the lee waves triggered clouds corresponding to the line-shaped precipitation bands over Osaka Bay.

The effects of latent heat release on the dynamics of mountain lee waves were examined with the aid of two-dimensional numerical simulations, for several situations in which the Scorer parameter had a nearly two-layer vertical structure (Durran and Klemp 1982). They showed that the steady waves were not produced in the conditionally unstable case. Condensation occurred in the crest of the first lee wave, but the cloudy regions were unstable and thus act as buoyant plumes. Our analyzed case is similar to their examined case.

Table 5.1. Local Froude number (*Fr*) of the windward air flowing toward the Shikoku Mountains for the four cases generating the Tokushima small low, computed in the hatched area shown in Fig. 2.6 using MANAL data. "–" indicates we cannot calculate Froude number because the wind direction is differ to southwest.

	09JST 12 July 2005	**09JST 2 July 2006**	**21JST 5 July 2006**	**09JST 21Jul 2006**
850 hPa	–	Fr = **2.34** h = 534 m $N = 1.4 \times 10^{-2}$ s^{-1}	Fr = **2.30** h = 579 m $N = 1.2 \times 10^{-2}$ s^{-1}	–
900 hPa	Fr = **1.01** h = 1013 m $N = 1.3 \times 10^{-2}$ s^{-1}	Fr = **1.31** h = 1027 m $N = 1.4 \times 10^{-2}$ s^{-1}	Fr = **0.95** h = 1075 m $N = 1.3 \times 10^{-2}$ s^{-1}	Fr = **1.32** h = 1058 m $N = 1.2 \times 10^{-2}$ s^{-1}
925 hPa	Fr = **0.97** h = 1252 m $N = 1.3 \times 10^{-2}$ s^{-1}	Fr = **1.30** h = 1265 m $N = 1.2 \times 10^{-2}$ s^{-1}	Fr = **0.90** h = 1314 m $N = 1.3 \times 10^{-2}$ s^{-1}	Fr = **1.08** h = 1292 m $N = 1.2 \times 10^{-2}$ s^{-1}
950 hPa	Fr = **1.03** h = 1485 m $N = 1.1 \times 10^{-2}$ s^{-1}	Fr = **1.34** h = 1497 m $N = 0.9 \times 10^{-2}$ s^{-1}	Fr = **0.92** h = 1548 m $N = 1.2 \times 10^{-2}$ s^{-1}	Fr = **0.86** h = 1532 m $N = 1.0 \times 10^{-2}$ s^{-1}

Chapter 6

General conclusion

On 2 and 5 July 2006, line-shaped precipitation bands (rainfall intensity > 30 mm h^{-1}) were formed around Osaka Bay. The width was 10 ~ 20 km, and the length was more than 100 km. They were maintained for 1 hour with moving eastward. We have demonstrated meso-β- and meso-γ-scale features near the cold front associated with meso-α-scale cyclone as follows (see Fig. 13).

1. Meso-α-scale cold front: Convectively (conditionally) unstable stratification (θ_e > 345 K at 950-hPa level, and ~335 K at 600-hPa level where moisture was less than 5 g kg^{-1}) appeared near the cold front passing Osaka Bay. The line-shaped precipitation band was generated in warm air in front of the cold front. It was located in the convergence zone between southwesterly from Kii Channel and westerly on the western (cold) side of cold front in the lower layer (below 900-hPa level). In the middle troposphere (~ 700-hPa level), strong westerly wind (20–30 m s^{-1}) corresponding to Baiu jet was also dominant over the precipitation band.
2. Meso-β-scale low ("Tokushima small low"): As the cold front approached Kinki District, a stationary meso-β-scale wave was formed from Shikoku Island to Kii Peninsula. In a trough of the wave located in the eastern part of Shikoku Island the Tokushima small low was generated and maintained for about 6 hours. The origin of the Tokushima small low is not considered to be thermal but hydrodynamic due to Shikoku Mountains. The warm moist southerly wind over Kii Channel was intensified (about 15 m s^{-1}) by the Tokushima small low in the lower layer (< 900-hPa level), and this southerly and the westerly corresponding to Baiu jet produced a vertical wind shear with clockwise rotation with height from surface to 700-hPa level. These are suitable for development of the line-shaped precipitation band.
3. Meso-γ-scale orographic effect: Westerly in the western side of the cold front passed over the meso-γ-scale mountains of Awaji Island and caused lee waves. The meso-γ-scale lee waves triggered active precipitation clouds in the conditionally unstable atmosphere produced by the conditions 1 and 2.

All of these conditions must be satisfied for generation of the line-shaped precipitation around Osaka Bay. Although cold fronts passed 15 times over Osaka Bay during 2003–2007, the line-shaped precipitation band appeared only two times. Such conditions in the present case are more complex than in the cases of heavy rainfall around Kyusyu Island, but may be similar to cases in other areas (from Shikoku Island to Kii Peninsula) in southern Japan. We are going to extend similar observational studies for these areas, and also to carry out numerical experiments removing of Shikoku and Awaji Islands.

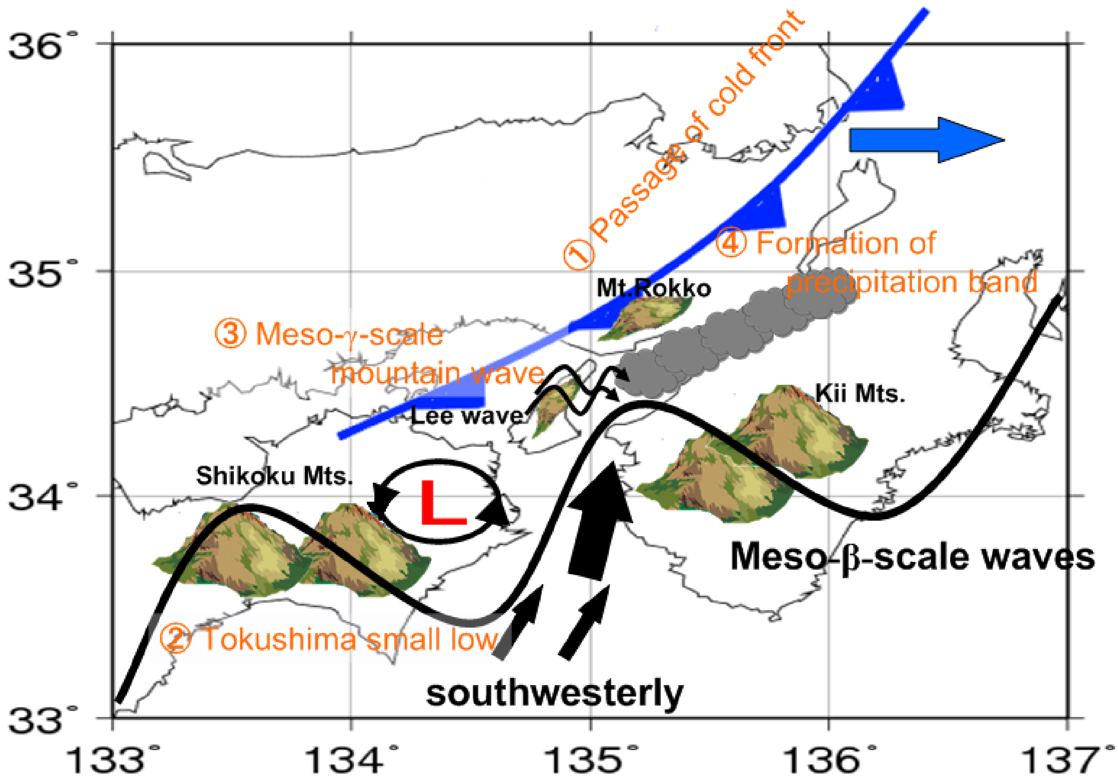

Figure 6.1. Schematic illustration in horizontal distribution of line-shaped precipitation band and environmental field. Thick arrows are wind at 900-hPa level. The solid wave line is mesoscale wave along southern coast and thin arrows are mountain wave.

References

Alexander, G.D. and G. S. Young, 1992: The relationship between EMEX mesoscale precipitation feature properties and their environmental characteristics. *Mon. Wea .Rev.*, **120**, 554-564.

Beebe, R.G. and F.C. Bates, 1955: A mechanism for assisting in the release of convective instability. *Mon. Wea. Rev.*, **83**, 1-10.

Durran, D.R. and J.B. Klemp, 1982: The effects of moisture on trapped mountain lee waves. *J. Atmos. Sci.*, **39**, 2490-2506.

Grell, G.A., J. Dudhia, and D.R. Stauffer, 1994: A description of the Fifth-Generation Penn State/NCAR Mesoscale Model (MM5). *NCAR Tech. Note*, NCAR/TN-398+STR, 122pp.

Hashiguchi, H., S. Fukao, Y. Moritani, T. Wakayama, and S. Watanabe, 2004: A Lower troposphere radar: 1.3-GHz active phased-array type wind profiler with RASS. *J. Meteor. Soc. Japan*, **82**, 915-931.

Higashi, K. and T. Fujii, 2004: A case study on local heavy rainfall observed in Kyoto city on 15 October 1998. *Acta Humanistica et Scientifica Universitatis Sangio Kyotiensis, Nat. Sci. Ser.*, **33**, 86-103 (in Japanese)

Higashi, K. and T. Fujii, 2008: Environmental characteristics of formation of line-shaped precipitation systems in passage of cold fronts in the Keihanshin area in 1999. *Acta Humanistica et Scientifica Universitatis Sangio Kyotiensis, Nat. Sci. Ser.*, **37**, 81-93 (in Japanese).

Higashi, K., Y. Kiyohara, M.D. Yamanaka, Y. Shibagaki, M. Kusuda and T. Fujii, 2009: Multiscale features of line-shaped precipitation band generation in central Japan during late Baiu season. *J.Meteor. Soc. Japan.,* submitted.

Hobbs, P.V., T.J. Matejka, P.H. Herzegh, J.D. Locatelli and R.A. Houze, Jr., 1980: The meso-scale and microscale structure and organization of clouds and precipitation in mid-latitude cyclones. I: A case study of a cold front. *J. Atmos. Sci.*, **37**, 568-596.

Hong, S.-Y., and H.-L. Pan, 1996: Nonlocal boundary layer vertical diffusion in a Medium-Range Forecast model. *Mon. Wea. Rev.*, **124**, 2322-2339.

Ishihara, M., Y. Kato, T. Abo, K. Kobayashi, and Y. Izumikawa, 2006: Characteristics and performance of the operational wind profiler network of the Japan Meteorological Agency. *J. Meteor. Soc. Japan*, **84**, 1085-1096.

Johnson, R.H. and P.J. Hamilton, 1988: The Relationship of surface pressure features to the precipitation and airflow structure of an intense mid-latitude squall line. *Mon. Wea. Rev.*, **116**, 1444-1472.

Kain, J.S., and J.M. Fritsch, 1990: A one-dimensional entraining/detraining plume model and its application in convective parameterization. *J. Atmos. Sci.*, **47**, 2784-2801.

Kato, T., 2005: Statistical study of band-shaped rainfall systems, the Koshikijima and Nagasaki lines, observed around Kyusyu Island, Japan. *J. Meteor. Soc. Japan*, **83**, 943-957.

Kato, T., 2006: Structure of the band-shaped precipitation system inducing the heavy rainfall observed Northern Kyushu, Japan on 29 June 1999. *J. Meteor. Soc. Japan*, **84**, 129-153.

Kato, T. and K. Aranami, 2005: Formation factors of 2004 Niigata-Fukushima and Fukui heavy rainfalls and problems in the predictions using a cloud-resolving model. *SOLA*, **1**, 1-4.

Kato, T. and H. Goda, 2001: Formation and maintenance processes of a stationary band-shaped heavy rainfall observed in Niigata on 4 August 1998. *J. Meteor. Soc. Japan*, **79**, 899-924.

Kato, T., M. Yoshizaki, K. Bessho, T. Inoue, Y. Sato, and X-BAIU-01 observation group, 2003: Reason for the failure of the simulation of heavy rainfall during X-BAIU-01 -Importance of a Vertical Profile of Water Vapor for Numerical Simulations-. *J. Meteor. Soc. Japan*, **81**, 993-1013.

LeMone, M.A., E.J. Zipser, and S.B. Trier, 1998: The role of environmental shear and thermodynamic conditions in determining the structure and evolution of mesoscale convective systems during TOGA COARE. *J. Atmos. Sci*., **55**, 3493-3518.

Metejka, T.J., R.A. Houze, Jr. and P.V. Hobbs, 1980: Microphysics and dynamics of clouds associated with mesoscale rainbands in extratropical cyclones. *Quart. J. R. Met. Soc*., **106**, 29-56.

Mohri, K.., 1956: An aerological study of heavy rainfall over west and central Japan during early summer 1953. *J. Meteor. Soc. Japan*, **34**, 244-253.

Ninomiya, K., 1978: Heavy rainfalls associated with frontal depression in Asian subtropical humid region (I) Synoptic scale features. *J. Meteor. Soc. Japan*, **56**, 253-266.

Ninomiya, K. and T. Akiyama, 1974: Band structure of mesoscale echo clusters associated with low-level jet stream. *J. Meteor. Soc. Japan*, **52**, 300-313.

Ninomiya, K. and T. Akiyama, 1992: Multi-scale features of Baiu, the summer monsoon over Japan and the East Asia. *J. Meteor. Soc. Japan*, **70**, 477-495.

Ninomiya, K. and Y. Shibagaki, 2007: Multi-Scale features of the Meiyu-Baiu front and associated precipitation systems. *J. Meteor. Soc. Japan*, **85B**, 103-122.

Ogino, S.-Y., M.D. Yamanaka and S. Fukao, 1999: Interannual and day-to-day variations of gravity wave activity in the lower stratosphere over the eastern part of Japan observed in winter 1989-95. *J. Meteor. Soc. Japan*, **77**, 413-429.

Ogura, Y., 1991: Analysis and mechanism of intense precipitation. *Tenki*, **38**, 276-288 (in Japanese).

Ogura, Y., 1997: Basic theory of Meso meteorology. *University of Tokyo Press*, 215pp (in Japanese).

Ogura, Y. and D. Portis, 1982: Structure of the cold front observed in SESAME-AVE III and its comparison with the Hoskins-Bretherton frontgenesis model. *J. Atmos. Sci.*, **39**, 2773-2792.

Orlanski, I., 1975: A rational subdivision of scales for atmospheric processes. *Bull. Amer. Meteor. Soc*., **56**, 527–530.

Reisner, J., R.M. Rasmussen, and R.T. Bruintjes, 1998: Explicit forecasting of supercooled liquid water in winter storms using the MM5 mesoscale model. *Quart. J. R. Met. Soc*., **124**, 1071-1107.

Sakakibara, H., 1983: Meso- and small-scale structure of a Cold-frontal precipitation system affected by a small low and mesoscale orography. *Pap. Meteorol. Geophys.*, **34**, 61-73.

Shibagaki, Y., M.D. Yamanaka, S. Shimizu, H. Uyeda, A. Watanabe, Y. Maekawa, and S. Fukao, 2000: Meso-β to -γ-scale wind circulations associated with precipitation clouds near Baiu front observed by the MU and meteorological radars. *J. Meteor. Soc. Japan*, **78**, 69-91.

Smolarliewicz, P.K., and R. Rotunno, 1989: Low Froude number flow past three-dimensional obstacles. Part I: Baloclinically generated lee vortices. *J. Atmos. Sci.*, **46**, 1154-1164.

Smolarliewicz, P.K., and R. Rotunno, 1990: Low Froude number flow past three-dimensional obstacles. Part II: Upwind flow reversal zone. *J. Atmos. Sci.*, **47**, 1498-1511.

Tashiro, S., 2004: Band-shaped precipitation system on the lee side of Koshikijima Islands revealed from radar observation. *Tenki*, **51**, 163-168 (in Japanese).

Tatehira, R. and H. Fukatsu, 1963: Radar and meso-scale analysis of a Cold front. *Tenki*, **41**, 145-157 (in Japanese).

Umemoto, Y., M. Teshiba, Y. Shibagaki, H. Hashiguchi, M.D. Yamanaka, and S. Fukao, 2004: Combined wind profiler-weather radar observations of orographic rainband around Kyushu, Japan in the Baiu season. *Ann. Geophys*., **22**, 3971-3982.

Ushijima, T., 1969: Analytical study of the low-level jet stream. *J. Meteor. Soc. Japan*, **47**, 13-22.

Yamakawa, S., 1980: Analysis of the heat-frontal thunderstorm accompanied by a cold front in Central Japan. *Tenki*, **27**, 735-742 (in Japanease).

Yamanaka, M.D. , S.-Y. Ogino, S. Kondo, T. Shimomai, S. Fukao, Y. Shibagaki, Y. Maekawa and I. Takayabu, 1996: Inertio-gravity waves and subtropical multiple tropopauses: Vertical wavenumber spectra of wind and temperature observed by the MU radar, radiosondes and operational rawinsonde network. *J. Atmos. Terr. Phys.*, **58**, 785-805.

Yoshizumi, S., 1977: On the structure of Intermediate-scale disturbances on the Baiu front. *J. Meteor. Soc. Japan*, **55**, 107-120.

Wang, C.-C. and G.T.-J. Chen, 2003: On the formation of leeside mesolows under different froude number flow regime in TAMEX. *J. Meteor. Soc. Japan*, **81**, 339-365.